Endopiriform neurons projecting to ventral CA1 are a critical node for recognition memory

Naoki Yamawaki[1,2,3], Hande Login[1,2,3], Solbjørg Østergaard Feld-Jakobsen[1], Bernadett Mercedesz Molnar[1], Mads Zippor Kirkegaard[1], Maria Moltesen[1], Aleksandra Okrasa[1], Jelena Radulovic[1,2,3,4,5] and Asami Tanimura*[1,2,3]

1. Department of Biomedicine, Aarhus University, Aarhus C, Denmark

2. PROMEMO, The Center for Proteins in Memory, Aarhus University, Aarhus C, Denmark

3. DANDRITE, The Danish Research Institute of Translational Neuroscience, Aarhus University, Aarhus C, Denmark

4. Dominick P. Purpura Department of Neuroscience, Albert Einstein College of Medicine, New York, USA

5. Department of Psychiatry and Behavioral Sciences, Albert Einstein College of Medicine, New York, USA

*Correspondence: Asami Tanimura (asami.tanimura@biomed.au.dk)

Abstract

The claustrum complex is viewed as fundamental for higher order cognition; however, the circuit organization and function of its ventral subregion, the endopiriform (EN), are not well understood. Using circuit analyses in mice, we show that EN neurons defined by their projection to ventral CA1 ($EN^{vCA1\text{-}proj.}$ neurons) were a major source of afferents to ventral CA1 (vCA1), with diverging collaterals to the olfactory-limbic system, and formed recurrent circuits within EN and with the piriform cortex. In vCA1, these axons exclusively targeted the distal subregion triggering potent feedforward inhibition of pyramidal neurons. By combining *in vivo* neuronal activity monitoring, circuit manipulations, and behavior analysis, we found that, during all phases of recognition memory test, the $EN^{vCA1\text{-}proj.}$ activity correlated with the time mice spent in particular arena locations. The $EN^{vCA1\text{-}proj.}$ activity was biased around social or non-social stimuli when they were present, especially when they were novel, a pattern consistent with salience detection and attention. Inhibition of $EN^{vCA1\text{-}proj.}$ neurons disrupted mice's memory-guided response to novel relative to familiar stimuli, without affecting innate bias for novel stimuli. These findings suggest EN as an essential node for social and object recognition memory, most likely by responding to salient environmental stimuli and by coordinating this response with downstream limbic system.

Introduction

The claustrum complex, an evolutionarily conserved brain region found across mammalian species, reptiles, and birds, is hypothesized to serve as a node for establishing higher order cognitive functions by coordinating neuronal activity on a global scale [1-3]. This view is based on its extensive connections with many cortical and subcortical areas [4,5]. Some of these functions include sensory perception and attention, which affects memory processing [6,7]. Consistent with this view, abnormalities of the claustrum complex is found in major cognitive disorders, including Alzheimer's disease, schizophrenia, and attention-deficit/hyperactivity disorder (ADHD) [8-10].

The cytoarchitecture and genetic expression broadly divide the claustrum complex into dorsal and ventral parts, with the dorsal part typically referred to as "claustrum" and ventral part having its own nomenclature: "endopiriform (EN)" in rodents [11,12]. Current evidence indicates that the claustrum forms reciprocal connections with dorsal cortices containing sensory, motor and association areas generating diverse physiological effects depending on the cortical targets and their activity patterns [4,5]. In contrast, EN primarily provides inputs to the piriform cortex and limbic systems [13,14], suggesting its distinct circuit organization and role in bridging olfactory information processed by the piriform cortex and memory processed by the limbic systems [15,16]. Nevertheless, many of the unique features of EN, such as circuit organization and function, have remained unclear.

One of distinct targets of EN, the ventral CA1 (vCA1), is known to coordinate in a range of behaviors related to exploration and recognition memory, and these functions are thought to be regulated by its afferent inputs in a domain-specific manner [17-23]. We, therefore, set out to characterize circuit and function of EN neurons defined by their projection to vCA1 ($EN^{vCA1\text{-}proj.}$ neurons) using genetic tools and mouse models of social and object recognition memory, and determine whether EN supports discrete domains of vCA1 functions (i.e., social versus object recognition) or more generic cognitive functions ascribed to claustrum complex.

We found $EN^{vCA1\text{-}proj.}$ neurons innervated selective components of the limbic system and produced potent feedforward inhibitory control over vCA1 pyramidal neurons. During recognition memory test, activity of $EN^{vCA1\text{-}proj.}$ neurons were condensed around conspecifics or objects where mice spent most time on. However, disruption of $EN^{vCA1\text{-}proj.}$ activity only impaired memory-guided exploration of novel stimuli without affecting innate exploration induced by novelty. These findings demonstrate that EN subserves some of the key functions required for recognition memory governed by specific limbic system.

Results

Endopiriform represents a major afferent of the ventral CA1

To assess the significance of EN as a vCA1 afferents, we injected a retrograde tracer into the vCA1 of mice and compared the number of the retrogradely labeled neurons in the EN and other brain regions (**Fig. 1a, b**, **Methods**). We found labeled neurons in multiple areas including the septum, entorhinal cortex, and basolateral amygdala (**Fig. 1c-f and Fig. S1a**) [24,25]. In addition to these well-known vCA1 afferents, prominent labeling was observed in the area defined as EN in Allen Brain Atlas (**Fig. 1g, Methods**). The number of presynaptic neurons in EN was ~10 fold lower than entorhinal cortex (data not shown). However, the normalized cell number of presynaptic neurons in EN was significantly greater than basolateral amygdala, lateral septum, and medial septum (**Fig. 1h**).

The vCA1-projecting neurons in the EN were spread along antero-posterior axis with two peak densities, one in anterior and another in posterior to the bregma (**Fig. 1i, j**). Number of labeled neurons was greater in posterior EN (**Fig. 1j**). In contrast, the same analysis along dorso-ventral axis showed a single dominant peak at the depth consistent with the location of EN (**Fig. S1b**).

To further confirm the location of these vCA1-projecting neurons, we injected a retrograde tracer in one color into vCA1 and a retrograde tracer in another color into a cortical area known to receive projections from EN or "claustrum" representing a dorsal part of claustrum complex (**Fig. 2a**). We targeted the prefrontal cortex to label EN, and the anterior cingulate cortex, the motor cortex, and the dorsomedial entorhinal cortex to label claustrum (**Fig. 2c-f**) [26-29].

We found there is a major spatial overlap in labeling of vCA1-projecting neurons with prefrontal cortex-projecting neurons, but not with other cortical projection neurons (**Fig. 2g-j**). Moreover, around 30% of vCA1-projecting neurons were found to be double-labelled when a cortical injection was made into the prefrontal cortex, suggesting some vCA1-projecting neurons send axons to this cortical area (**Fig. 2k, l**).

To further determine the cortical and subcortical innervation pattern of vCA1-projecting EN neurons, we used an intersectional approach to label their somata and axons with eGFP (**Fig. 2m**). Apart from vCA1, axons from vCA1-projecting neurons were found in various cortical areas including prefrontal cortex, lateral entorhinal cortex, and piriform cortex (**Fig. 2n-p and Fig. S2a-c**). Projection to prefrontal cortex was sparse relative to other areas, as expected based on the retrograde labeling data (**Fig. 2k**). The connectivity of vCA1-projecting EN neurons to the amygdala, which represents the major component of limbic systems, was also sparse relative to vCA1 (**Fig. S2c**), indicating vCA1 is the main target of these EN neurons in this system.

Taken together, these findings indicate EN represents a major afferent of vCA1. Moreover, EN neurons projecting their axons to vCA1 also send strong collaterals to lateral entorhinal cortex and piriform cortex, but relatively weak to the prefrontal cortex or other limbic structures. Since our subsequent study focused on EN neurons defined by their projection to vCA1, we refer to them as $EN^{vCA1\text{-}proj.}$ neurons.

Projection pattern and synaptic connectivity of EN axons in vCA1

We next investigated projection pattern of EN axons in hippocampus by injecting an anterograde tracer (AAV-GFP) into the EN (**Fig. 3a, b**). Analysis of different parts of hippocampal section indicated EN axons were mostly confined in stratum lacunosum-moleculare (SLM) layer of distal part of vCA1 (**Fig. 3c, d**). Projection to intermediate or dorsal CA1 was limited or undetectable (**Fig. S3a-c**).

Since SLM mainly consists of GABAergic neurons [30], we hypothesized that EN axons form synapses with this cell type. To test this, we first applied monosynaptic rabies tracing technique to Vgat-Cre mice (**Fig. 4a, Methods**). The distribution of starter cells (identified by GFP and mCherry co-labeling) was confirmed to be within the ventral-intermediate region of hippocampus using AMaSiNe (**Fig. 4b, S4a**) [31]. In these mice, the presynaptic neurons were consistently observed in EN in addition to other expected areas (e.g., septum and entorhinal cortex) (**Fig. 4c and d, S4b-f**) [32,33]. The density of the presynaptic neurons in EN was greater at the posterior region to the bregma (**Fig. 4d**), consistent with our earlier observation (**Fig. 1j**).

To determine how EN inputs are integrated into the local circuit in vCA1, we systematically assessed the connections between EN axons and GABAergic neurons in different layers of distal vCA1. We expressed channelrhodopsin-2 (ChR2) into the EN axons by injecting AAV-ChR2-mCherry into EN and performed whole-cell recording from GABAergic neurons in acute vCA1 slices in the presence of TTX (1 μM) and 4-AP (100 μM) to isolate monosynaptic connection [34]. To ensure the recording from GABAergic neurons, we used Vgat::Ai14 mice in which all GABAergic neurons are labeled with tdTomato (**Fig. 4e-g**). We recorded from 3 to 4 GABAergic neurons located in different laminar position in distal vCA1 (Py-SR border, SR, SR-SLM border, or SLM) in the same slice to construct a "laminar profile" of EN→vCA1 inputs (**Fig. 4f and g**). Whole-field LED stimulation evoked excitatory postsynaptic current (EPSC) in most GABAergic neurons recorded. However, contrary to

132 the expectation, connection probability and strength were lowest in neurons in SLM compared to
133 neurons in other layers (**Fig. 4h-j**).

134 Taken together, these results indicate EN axons preferentially innervate the GABAergic neurons
135 spanning across the Py-SR border to SR-SLM border in distal vCA1.

136 **EN axons produce feedforward inhibition onto vCA1 pyramidal neurons**

137 SLM also contains the apical tuft dendrite of pyramidal neurons, which could be a target of EN axons
138 in addition to GABAergic neurons. To test this, we expressed ChR2 in EN axons but made whole-cell
139 recording from pyramidal neurons in distal vCA1 in the presence of TTX and 4-AP. Since CA1
140 pyramidal neurons can be differentiated into superficial and deep layer neurons with distinct anatomy
141 and function [35], we recorded from neurons in each layer as well as nearby GABAergic neurons at the
142 Py-SR and SR-SLM borders for the comparison (**Fig. 5a**). We found monosynaptic input to
143 superficial and deep layer pyramidal neurons was similar, and monosynaptic input to pyramidal
144 neurons (superficial and deep pooled) and GABAergic neurons was also comparable (**Fig. S5**).

145 Since EN axons innervated multiple GABAergic neurons across different layers, we hypothesized
146 they may exert stronger inhibition onto pyramidal neurons through feed-forward inhibition. To test
147 this, we recorded EPSC and inhibitory postsynaptic current (IPSC) from superficial and deep
148 pyramidal neurons using cesium-based internal solution in the brain slices expressing ChR2 in the EN
149 axons (**Methods**). At the command potential of -70 mV, photo-stimulation of EN axons evoked
150 EPSCs in majority of pyramidal neurons in both layers (7 out of 10 neurons in superficial and 5 out of
151 10 neurons in deep) **(Fig. 5b**). At the command potential of +12 mV, the same stimulation evoked
152 outward postsynaptic current in the same neurons, including those without EPSCs (10 out of 10 for
153 superficial and deep) (**Fig. 5b**). This outward current was abolished by application of TTX and 4-AP
154 or gabazine (10 μM), indicating it is disynaptically driven and mediated by inhibitory $GABA_A$
155 receptor (**Fig. 5b**). When relative strength of EPSCs and IPSCs were compared for each neuron, the
156 strength of IPSCs overwhelmed the EPSCs in all cases (**Fig. 5c**). This indicates EN axons
157 disynaptically inhibit pyramidal neurons in vCA1 (**Fig. 5d**).

158 **$EN^{vCA1\text{-}proj.}$ neurons receive inputs from the piriform cortex**

159 We next examined afferents that may drive the EN→vCA1 circuit. To address this, retrograde CAV-
160 2-Cre was injected into vCA1 to express Cre into $EN^{vCA1\text{-}proj.}$ neurons, then applied monosynaptic
161 rabies tracing technique to specifically label its presynaptic neurons in wild type mice (**Fig. 6a**).
162 Starter cells and presynaptic neurons were spatially mapped and quantified using AMaSiNe (**Fig. 6b**
163 **and c, S6**). Since presynaptic neurons were sparse in contralateral hemisphere, data from ipsilateral
164 hemisphere was analyzed. Moreover, we applied minimum labeling threshold to determine the brain
165 region for further analysis (**Methods**). We found the piriform cortex contained highest number of
166 presynaptic neurons followed by EN (**Fig. 6d-f**). Within piriform cortex, layer 2 neurons were the
167 major source of afferent (**Fig. 6g**). These data indicate $EN^{vCA1\text{-}proj.}$ neurons receive major input from
168 piriform cortex and form a recurrent connection with neurons in EN (**Fig. 6h**).

169 **The activity of $EN^{vCA1\text{-}proj.}$ neurons is correlated with the time mice spend in space**

170 The downstream target of EN, vCA1, is implicated in social, odor and object recognition memory [19-
171 21]. To determine whether and how the activity of EN neurons is related to this function, we expressed
172 GCaMP8s in $EN^{vCA1\text{-}proj.}$ neurons and monitored their activity using fiber photometry while video
173 recording mice performing social recognition memory test consisting of pretest, sociability test, and
174 discrimination test (**Fig. 7a, b, Methods**). The nose position of the subject mouse was tracked during
175 tests using DeepLabCut (**Fig. 7c**) [36,37], and cumulative time and calcium event were mapped onto the
176 arena space (**Fig 7c, S7**). We found these values were correlated in space across all sessions (i.e., the

more time the mice spent in a given space, the more the $EN^{vCA1\text{-}proj.}$ activity), including in the open field with no object or in the test arena with conspecifics or objects (**Fig. S7, S8a-b**).

Cumulative calcium events of $EN^{vCA1\text{-}proj.}$ neurons became high towards the space around objects or conspecifics when they are present and was correlated with interaction times except for sociability session (**Fig. S8c-d**). In the sociability session, the cumulative calcium events around a novel conspecific and object were similar despite mice spending more time on conspecifics (**Fig. 7e left, S8c**). In contrast, in the social discrimination test, both the cumulative time and cumulative $EN^{vCA1\text{-}proj.}$ activity were higher for an unfamiliar than familiar conspecific (**Fig. 7d-e, S8c**). As a result, $EN^{vCA1\text{-}proj.}$ activity and behavior had a greater degree of correlation in social discrimination than sociability.

We also tested if a similar correlation occurs in a non-social context by recording $EN^{vCA1\text{-}proj.}$ activity and behavior in the object discrimination test (**Fig. 7f**). The cumulative time and calcium events were significantly correlated across different sessions i.e., familiarization, and object discrimination (**Fig. 7g, S8e**), largely consistent with the findings in the social discrimination test.

These data indicate that the activity of $EN^{vCA1\text{-}proj.}$ neurons is generally correlated with the time the mouse spends in a particular location at the basal level (i.e. open field) or task conditions. However, the degree of correlation appears to vary depending on the session, such that it was highest in the pretest/familiarization and social/object discrimination test, but lowest in the sociability test.

Inhibition of $EN^{vCA1\text{-}proj.}$ neurons impairs social/object recognition memory

Although $EN^{vCA1\text{-}proj.}$ activity predicted the behavior in pretest/familiarization and discrimination test better than sociability test, their causality is unclear. To address this, we inhibited the activity of $EN^{vCA1\text{-}proj.}$ neurons using inhibitory DREADD (hM4Di) during social and object discrimination tests (**Fig. 8a-c and h, S9a**) [38]. To specifically express hM4Di in $EN^{vCA1\text{-}proj.}$ neurons, CAV-2-Cre and AAV-flox-hM4Di were bilaterally injected into vCA1 and EN, respectively (**Fig. 8a-b**). hM4Di was replaced with tdTomato for control group. We made a protocol that allows within-subject comparison, such that a mouse goes through a test with chlozapine-N-oxide (CNO, 1 mg/ kg) treatment then the same test with saline treatment the next day, or vice versa (**Fig. 8c and h**). In social discrimination test, CNO treatment did not affect the pretest or sociability in hM4Di or control group, but specifically impaired social discrimination in hM4Di group (**Fig. 8d-g, S9b-c**). A similar effect was also observed in novel object discrimination (**Fig. 8i, S9d**).

Apart from recognition memory, vCA1 is implicated in anxiety and associative fear memory [39,40], thus, we tested contribution of $EN^{vCA1\text{-}proj.}$ neurons to these functions. The anxiety level as determined by locomotor activity and sociability was not affected by CNO treatment in hM4Di group (**Fig. 8e, S9e**). Similarly, fear memory as assessed by the freezing response during training (with trace fear conditioning) or recall to context or tone was not affected by CNO treatment in hM4Di group (**Fig. S10**).

Taken together, these data indicate that $EN^{vCA1\text{-}proj.}$ activity is not causally related to innate exploration behavior induced by novelty, or anxiety or fear memory. However, their activity is necessary for mice to discriminate between familiar and unfamiliar conspecific or object, suggesting their major role in general recognition memory.

Discussion

We characterized the circuit and function of EN neurons targeting specific subregions and layers of vCA1. In contrast to other parts of claustrum complex, $EN^{vCA1\text{-}proj.}$ neurons were reciprocally connected with the piriform cortex representing a major downstream target of the olfactory bulb [41]. This circuit motif may predict the predominant role of $EN^{vCA1\text{-}proj.}$ neurons in social recognition memory, given the ability of social odor to engage multiple olfactory pathways innervating the

222 piriform cortex [42]. However, we found that these neurons contributed to broader domains of
223 recognition memory. This is supported by the observations that the inhibition of $EN^{vCA1\text{-}proj.}$ activity
224 impaired both social and non-social discrimination.

225 In all phases of recognition memory test, $EN^{vCA1\text{-}proj.}$ activity was highly correlated with the time mice
226 spent in given locations and this correlation was biased towards novel stimuli when mice were
227 engaged in their exploration irrespective of the stimuli being social or non-social. Taken together,
228 these data suggest that the function of $EN^{vCA1\text{-}proj.}$ neurons was primarily related to the detection of and
229 attention to novel stimuli. The recurrent connections within EN, which is another prominent feature of
230 $EN^{vCA1\text{-}proj.}$ neurons' network, potentially support these processes to help establish the recognition
231 memory [43] (**Fig. 9**).

232 Attentional processes mediated by $EN^{vCA1\text{-}proj.}$ neurons can be considered of particular relevance for
233 memory-guided behavior, given that inhibition of $EN^{vCA1\text{-}proj.}$ activity selectively impaired
234 conspecific/object discrimination but not innate exploratory behavior provoked by novelty as seen in
235 pretest, sociability, and familiarization. This functional specialization, likely associated with its
236 unique circuit connectivity to the limbic system, could differentiate EN from claustrum.

237 Studies on EN are generally scarce, and the available evidence of EN projections to vCA1 suggests
238 that these projections are sparse [13]. Potential reasons include the difficulty in clearly delineating the
239 EN from claustrum complex and non-uniform distribution of $EN^{vCA1\text{-}proj.}$ neurons along antero-
240 posterior axis. By leveraging contemporary circuit analysis tools, we demonstrated that the
241 EN→vCA1 circuit is non-trivial; $EN^{vCA1\text{-}proj.}$ neurons were more numerous than commonly studied
242 vCA1 afferents, including those from the septum and amygdala. Moreover, these axons exhibited a
243 potent disynaptic inhibition of distal vCA1 pyramidal neurons, indicating their major functional
244 implications for vCA1 activity.

245 Our data indicated that although EN axons terminated at the SLM of distal vCA1, they exhibited
246 stronger connections to GABAergic neurons spanning from the Py-SR border to the SR-SLM border
247 than to SLM neurons. The detection of EN inputs from GABAergic neurons at the Py-SR border was
248 surprising, considering the distance between soma position and the EN axons. However, there are
249 several GABAergic cell types below SLM that extend their primary dendrites into SLM [44,45], likely
250 explaining the observed connectivity pattern. Among these are chandelier cells found at the Py-SR
251 border, which preferentially inhibits the axon initial segments of pyramidal neurons, and are thus well
252 suited to exert the powerful feedforward inhibition of vCA1 pyramidal neurons observed in our
253 recordings [46].

254 There are several potential circuit effects by which EN inputs could affect vCA1 function. One is the
255 induction of non-linear events in vCA1 pyramidal neurons by acting in concert with other afferents
256 (e.g., lateral entorhinal cortex targeting SLM) [33] to generate a specific output pattern in pyramidal
257 assemblies representing task-relevant stimuli. Alternatively, EN inputs may improve signal to noise
258 ratio of the information conveyed through the lateral entorhinal cortex, CA2 (in the case of social
259 context), and possibly other afferents (e.g., CA3) [47]. Another scenario is tuning of vCA1 pyramidal
260 neurons' response to familiar stimuli through dynamic combination of a weak monosynaptic
261 excitatory input and strong disynaptic inhibitory input. Such mechanism suggests that at a
262 milliseconds scale novelty (EN) and familiarity (vCA1) recognition might occur though alternating
263 rather than simultaneous activity of brain microcircuits.

264 The model of promoting novelty detection by suppressing familiarity responses is consistent with
265 previous observations showing that vCA1 pyramidal neurons predominantly respond to familiar
266 stimuli whereas novelty response can only occur through activation of vCA1 interneurons [48,49].
267 Nevertheless, alternating activation of EN and vCA1 could prove essential for the behavioral
268 relevance of EN activity associated with recognition memory, without affecting innate exploratory

behavior to novelty. Accordingly, the latter behavior is primarily associated with the prefrontal cortex and amygdala, areas that are only weakly targeted by $EN^{vCA1\text{-}proj.}$ neurons (**Fig. 2p, S2c**) [50-52].

In addition to advancing our understanding of the basic organization and function of brain circuits underlying higher cognitive processes, our findings suggest dysfunction of $EN^{vCA1\text{-}proj.}$ neurons could be a key contributing factor to the deficits in claustrum complex function and recognition memory found in neuropsychiatric disorders [8,9]. Discrete EN populations can thus emerge as pathophysiological substrate, but also as important treatment targets of key symptoms of these disorders.

Acknowledgement

We thank Wen-Hsien Hou, Chihiro Nakamoto, Ana Cicvaric, Hui Zhang, and Elizabeth Wood for constructive discussion of this study. We thank Peter Bjerge, Bjark B. Brix, and Dennis Olesen for technical help. We acknowledge the bioimaging core facility, Health, Aarhus University, Denmark, for the use of equipment and support. This research is funded by LF professorships to J.R. (R310-2018-3611), and LF experiment to N.Y. (R436-2023-471), and A.T. (R436-2023-855).

Methods and materials

Mice

All experiments were performed in accordance with standard ethical guidelines and were approved by the Danish national animal experiment committee (License number: 2021-15-0201-00801). Unless otherwise noted, all mice used were C57BL6/J mice or transgenic mice with C57BL6/J backgrounds. They were 2-4 months old at the time of the experiment. Transgenic mice used were B6.Cg-Gt (ROSA)26Sor$^{tm14(CAG\text{-}tdTomato)Hze}$/J mice (Ai14, JAX007914) and B6J.129S6(FVB)-Slc32a1$^{tm2(cre)Lowl}$/MwarJ mice (Vgat-Cre, JAX028862). Similar number of male and female mice were used for all experiments except for behavior tests. For behavior tests, male mice were used.

Viruses and retrograde tracers

The information on viruses used in our experiments was the following. CAV-2-Cre (PVM); AAV1-mDlx-HBB-chl-dlox-TVA_2A_oG(rev)-dlox (v271-1, VVF); AAV1-hSyn1-dlox-TVA_2A_mCherry_2A_oG(rev)_dlox (v306-1, VVF); Rabies-GFP (NTNU viral core facility); Rabies-mCherry (NTNU viral core facility); AAV5-CAG-GFP (37525-AAV5, Addgene); AAV5-CAG.hChR2(H134R)-mCherry (10054-AAV5, Addgene); AAV8-hSyn-DIO-hM4Di (Gi) –mCherry (44362-AAV8, Addgene); AAV5-hEF1a-dlox-EGFP(rev)-dlox (v217-5, VVF); and retrograde AAVrg-CAG-GFP (37825-AAVrg, Addgene), AAV1-hSyn1-dlox-jGCaMP8s(rev) (v627-1, VVF). We also used retrograde traces of red Retrobeads (Lumafluor) and Cholera toxin subunit B conjugated with Alexa 647 (CTB647, Thermo Fisher).

Stereotaxic injections

Stereotaxic injections were performed using a stereotaxic frame (Model 940, Kopf). Mice were anesthetized with isoflurane and were subcutaneously injected with buprenorphine (0.1 mg/kg) and metacam (1.5 mg/Kg) for post-operative pain relief. After incising the scalp over the cranium, a small hole was bored with a microdrill bit, and a beveled glass pipette (Wiretrol II, 5-000-2010, Drummond Scientific Company) back-filled with mineral oil and front-filled with the material to be injected was slowly inserted into a target coordinate. After injecting a small volume (50 - 100 nL) with a custom-made displacement injector (based on MO-10, Narishige), the pipette was left in place for 3 to 5 mins before slow retraction. The incision was closed with a nylon suture. The stereotaxic coordinates used were (relative to bregma, in mm): anteroposterior (AP) -3.0; mediolateral (ML) 3.12; dorsoventral (DV) 3.7 for ventral CA1; AP +2.0; ML 0.2; DV 1.5 and 2.5 for prefrontal cortex; AP 0.0; ML 0.2; DV 1.0 and 1.5 for anterior cingulate cortex; AP 0.0; ML 1.5; DV 0.3 and 0.7 for motor cortex; and

314 AP -5.0; ML 3.0; DV 1.5 for dorsomedial entorhinal cortex. For endopiriform injection, we injected
315 two sites from the following coordinates: AP -0.27, ML 3.2, DV 4.2; AP 0.0, ML 3.0, DV 4.2; or AP
316 +1.0, ML 2.7, DV 4.0. Mice were thermally supported with a feedback-controlled heating pad
317 maintained at ~37 ºC (ThermoStar Homeothermic system, RWD). Mice were used for experiments 3-
318 5 weeks post injection.

319 **Implantation of the optic probe**

320 After stereotaxic injection of CAV-2-Cre into the vCA1 and AAV1-hSyn1-dlox-jGCaMP8s into the
321 EN (AP -0.27, ML 3.2, DV 4.2), a fiber optic cannula (400 µm core diameter, 4.5 mm length, NA
322 0.39, R-FOC-BF-400C-39NA, RWD) was inserted towards EN. Once in the correct depth, exposed
323 brain surface around the implant was covered by Kwik-Cast (WPI) and was then fixed on skull with
324 dental adhesive resin cement (Super-Bond, SUN MEDICAL).

325 ***Ex vivo* electrophysiology**

326 Mice were deeply anesthetized with isoflurane and decapitated. Horizontal sections (300 µm)
327 containing ventral hippocampus were prepared by vibratome (VT1200S, Leica) in ice-cold choline
328 solutions containing (in mM): 25 $NaHCO_3$, 1.25 NaH_2PO4-H_2O, 2.5 KCl, 0.5 $CaCl_2$, 7 $MgCl_2$, 25 D-
329 glucose, 110 Choline chloride, 11.6 Ascorbic acid, and 3.1 $C_3H_3NaO_3$. Slices were subsequently
330 incubated in artificial cerebrospinal fluid (ACSF) containing (in mM): 125 NaCl, 25 $NaHCO_3$, 1.25
331 NaH_2PO4-H2O, 2.5 KCl, 11 D-glucose, 2 $CaCl_2$, and 1 MgCl at 34 ºC for 30 mins then at room
332 temperature (~20 ºC) for at least 1 hour before the recording.

333 Whole-cell recording was performed with an upright microscope (BX51WI, Olympus) equipped with
334 a motor-controlled stage and focus (MP285A and MPC-200, Sutter instrument), differential
335 interference contrast, coolLED (model pE300), and a monochrome camera (Moment, Teledyne).
336 Neurons were visualized with a 60x lens (1.00 NA, LUMPlanFL N, Olympus) with the software
337 Micro-Manager-2.0 gamma (US National Institutes of Health). Pipettes (4-5 MΩ) were pulled from
338 thick-walled borosilicate capillary glass with a puller (model P-1000, Sutter instrument). For a
339 voltage-clamp recording, the internal solution contained (in mM): 135 $CsMeSO_3$, 10 HEPES, 4 Mg-
340 ATP, 0.3 Na-GTP, 8 Na_2-Phosphocreatine, 3.3 QX-314 (pH was adjusted to 7.35 with CsOH). In
341 some experiments, a biocytin (4 mg/mL) and Alexa488/586 (50 µM) were further added for
342 morphological studies. Recordings and hardware control were performed with Wavesurfer (Janelia
343 Farm). Signals were amplified and Bessel filtered at 4 kHz with an amplifier (MultiClamp 700B,
344 Molecular Device), then sampled at 10 kHz with a data acquisition board (USB-6343, National
345 Instrument). Recording with access resistance change of > 20% from the baseline (~30 MΩ or less)
346 were discarded. Liquid junction potential was not corrected. All recordings were performed at ~34 ºC
347 maintained with the inline heating system (TC-324C, Warner instrument).

348 To stimulated channelrhodopsin-2, a blue LED was delivered at a short pulse (5-msec) through a 4x
349 objective lens (0.16 NA, UPlanSApo, Olympus). The light power (measured at the focal plane) was
350 20 mW for the recordings in normal ACSF and 40 mW for the recordings in the presence of
351 tetrodotoxin and 4-aminopyridine. Photo-stimulation was repeated 3 to 6 times (at intervals of 10 or
352 20 sec) to obtain an average response trace. Photo-evoked responses less than 2 standard deviations of
353 the baseline were considered as a "zero" response. The mean amplitudes indicate mean amplitudes
354 between LED stimulus-onset to 50 ms of average responses.

355 **Quantification of presynaptic neurons**

356 Mice were deeply anaesthetized with a ketamine (120 mg/kg) and xylazine (24 mg/kg) mixture and
357 were transcardially perfused with 4% paraformaldehyde (PFA). The brains were extracted and
358 immersed in 4% PFA overnight followed by 20 and 30% sucrose solution for a cryoprotection. The
359 brains were subsequently embedded in O.C.T compound (Tissue TEK, Sakura) in a mold and frozen

360 on the dry ice. Coronal slices (100 µm) of entire brain were cut with Cryostat (CM3050S, Leica) and
361 were washed with phosphate-buffered saline (PBS) before DAPI staining. All sections were mounted
362 onto glass slides with a coverslip (thickness:0.13-0.17 mm, Hounisen) and mounting media (DAKO,
363 S3023, Agilent Technologies).

364 The injection sites and its specificity were verified by registering the images into Allen Brain atlas
365 using QuickNII and VisuAlign [53].

366 For quantification of presynaptic neurons and visualization of their distribution in 3D mouse brain,
367 epifluorescence images acquired with Slidescanner (4231 x 3462 pixels, 10x objective, Olympus
368 VS120) were analyzed with Matlab-based program AMaSiNe [31]. For **Fig.1**, the coronal section
369 between AP + 3 to -4 mm were registered in AMaSiNe and analyzed.

370 For the monosynaptic rabies tracing study in **Fig. 6**, the brain areas containing over 1% presynaptic
371 cells of total presynaptic cells were proceeded further analysis. Fraction of presynaptic cells in the
372 different areas were calculated by dividing a number of presynaptic cells in each brain areas by the
373 average number of presynaptic neurons in all brain areas.

374 For the study in **Fig. 2**, the sections were immunostained with NeuN before imaging. Here, sections
375 were immersed with 5% normal goat serum and 0.2% Triton X for 30 mins at room temperature
376 before incubation with NeuN primary antibody (anti-rabbit, 1:1000) (ABN78, Milipore) at 4 ºC for
377 overnight. The sections were then washed with PBS and were further incubated with secondary
378 antibody (goat anti-rabbit conjugated with Alexa 488 or 568, 1:500) (A11008 or A11036, Thermo
379 Fisher) for 1 hour at room temperature before mounting. A single plane image of claustrum complex
380 was acquired with confocal microscope (10x objective, 1024 x 1024 pixels, Zeiss). 2-4 images, range
381 of AP: +1.4 to -0.2, were collected per brain. Fraction of double-labelled neurons (with different
382 retrograde tracers) were calculated for each brain by dividing a total number of double-labeled
383 neurons by the total number of vCA1-projecting neurons (labeled with one color).

384 **Quantification of fluorescence signal from axons**

385 For **Fig. 3 and S3**, horizontal section (100 µm) images were taken with Sliderscanner (10x lens, pixel:
386 2560 x 3072). All images from the same brain were taken with the same light intensity and detection
387 setting. After background subtraction, GFP signals in ventral, intermediate, and dorsal CA1 column
388 were normalized by the highest signal in ventral CA1 in the same brain.

389 For **Fig. 2**, coronal sections (100 µm) were immunostained with GFP antibody before imaging. Here,
390 sections were washed with PBS, the sections were incubated in blocking solution containing 5%
391 normal goat serum and 0.2% Triton X for 30 mins at room temperature before incubation with GFP
392 primary antibody (anti-rabbit, 1:1000) (NB600-308, MNovus Biologicals) in blocking solution at 4 ºC
393 for overnight. The sections were then washed with PBS and were further incubated with secondary
394 antibody (goat anti-rabbit conjugated with Alexa 488, 1:300) (A11008, Thermo Fisher) for 1 hour at
395 room temperature before mounting. Images were taken with Slidescanner (10x, pixel: 3072 x 3584).
396 Signal per pixel in ROI was calculated for each projection site after background subtraction.

397 **Social memory test with chemogenetic inhibition of $EN^{vCA1\text{-}proj.}$ neurons**

398 Social memory test is based on previous articles with slight modifications [54, 55]. All tested mice were
399 habituated to the handling for 3 days. Prior to the test day, we divided subject mice into two groups.
400 On the 1st test day (session 1), one group received chlozapine-N-oxide (CNO, 1 mg/kg, i.p.) and
401 another group received a vehicle. After 30 mins, the subject mice were placed in a three-chamber box
402 for 5 mins (habituation), then the same box with two pencil chambers containing the same object in
403 opposite corners for 5 mins (pretest). After 5 mins break in their home cage, the subject mice were
404 again placed in the same box, but this time, an object in one pencil chamber was replaced with

different object and an object in another pencil chamber was replaced with a conspecific (3-4 weeks old male, habituated to the handling and pencil chamber for 3 days prior to the session 1). This "sociability test" lasted for 10 mins and was followed by social discrimination test after 30 mins break in the home cage. The social discrimination test lasted for 5 mins and consisted of the same setting as the sociability test except an object in a pencil chamber, which was replaced with a new conspecific (i.e., a novel mice). In the following day, CNO and saline treatments were swapped between the groups, and all mice went through the same series of tests (session 2) for the within-subject comparison of the CNO effect. The position of the pencil chamber including an object or a conspecific were counterbalanced. The tests were performed under 6-10 lx room light and video was recorded at 25 frames/sec with GigE camera (Basler ace acA1300-60gm, Basler) placed at the ceiling.

Trace fear conditioning

After one week of social memory test, subject mice were examined for their tone-associated fear memory and extinction. One group received CNO while another group received vehicle 45 mins before the test. In conditioning day, mice were placed in a box with a metal grid floor and ethanol odor (context A) and after 3 mins were delivered with 20-sec pure tone (2 kHz, 20 dB) followed by 18-sec time gap (trace) and 2-sec footshock (0.5 mA). The exposure to the same tone-trace-shock sequence was repeated 2 more times with inter-trial interval of 2 mins. In the following day, mice were re-exposed to the context A for 3 mins to assess their fear memory to the context. From day 3, mice were placed in a new context, the context B (smooth floor, breach odor), and went through the same protocol as in conditioning day but without shocks. The process was repeated over 5 days to assess the extinction of the fear memory to the tone and trace. All test was performed in dark (but infrared light was on), and behavior was video recorded at 25 frames/sec with infrared GigE camera (Basler ace acA1300-60gm, Basler).

Novel object recognition test

The novel object recognition test is based on the previous article with slight modifications [54]. The subject mice were divided into two groups and CNO treatment was done as same as social memory test. 40 mins after CNO/vehicle i.p. injection, the subject mice were placed in an open field box (50 x 50 cm) for 5 mins (habituation). In following familiarization session, two same shape objects are placed in the open field box, and then the subject mice explored for 10 mins. After 1 hour break in their home cage, the subject mice were again placed in the same box, but one object is replaced by a novel object. The subject mice are allowed to explore the box for 5 min in discrimination session.

Social memory test and novel object recognition test with *in vivo* fiber photometry

Optic probe implanted mice were habituated handling for 3 days prior the test. In test day, the subject mouse attached with patch code were placed in an open field box (50 x 50 cm) for 5 min (habituation). After habituation, the mouse was place in a home cage for resting and waiting following session. For pretest, pencil chambers containing the same objects were placed at the corners of the open field box. Pretest was tested for 5 min. For sociability test, a novel mouse (4 weeks old, male) or a novel object were placed in pencil chambers. Sociability test took 10 min. After sociability test, the subject mouse return to a home cage and rest for 20 min. After 20 min rest, the subject mouse was tested discrimination session for 5 min. In discrimination test, a novel mouse (4 weeks old, male) or a familiar mouse that was used as the stimulus mouse in sociability test were placed in pencil chambers. Both in sociability and discrimination test, positions of pencil chambers were counterbalanced between subject mice. The tests were performed under 6-10 lux room light and video was recorded at 60 frames/sec with GigE camera (Basler ace acA1300-60gm, Basler) placed at the ceiling. Video acquisitions were controlled by Bonsai. Simultaneous start of video recording and calcium signal recording was controlled by Raspberry Pi.

After one week of social memory test, subject mice were examined for novel object recognition test. The procedure, the arenas and objects were used the same as in the novel object recognition test with chemogenetic inhibition of $EN^{vCA1\text{-}proj.}$ neurons.

Behavior data acquisition and analysis

Ethovision (version 16 or 17, Noldus) was used for the hardware control and data acquisition and initial quantification for the behavior. Behavioral variables, including movement trajectory, times spent in predefined areas, total distance traveled, travelling velocity, and freezing were extracted and further analyzed/nested with custom functions in the Matlab (R2020b). For social memory test, interaction zones were defined as an area between the edge of pencil chamber and 3 cm away from the edge. When the nose of the subject mouse was in the zone, the time was counted as interaction time. Sociability index was calculated by dividing total interaction time with mouse by total interaction time with mouse and object. The discrimination index was calculated by dividing total interaction time with a novel mouse by total interaction time with a familiar mouse and a novel mouse. Data from mice were excluded if discrimination index was less than 0.5 during saline treatment. For trace fear conditioning test, mice were considered "freezing" if pixel change between frames was less than 0.1 % for more than 1 sec.

Deeplabcut (ver.2.3) was used for tracking of annotated body points of the subject mice connected with patch code for calcium imaging of $EN^{vCA1\text{-}proj.}$ neurons during social memory test and novel object recognition test. Nose points were used for further analysis using Matlab (R2020b). To define interaction zone, reference points was set at the center of pencil chamber. The areas that distance between nose point and reference point was less than 100 pixel for social memory test and 50 pixel for novel object recognition test were dedicated to interaction zone.

Fiber photometry and analysis

Population activity of $EN^{vCA1\text{-}proj.}$ neurons were recorded using fiber photometry (Doric Lenses). GCaMP8s was excited with 470 nm light at 20-30 μW measured at the tip (isosbestic point used was 415 nm (15 μW)). Calcium-dependent and independent signals were collected using lock-in mode. Signals were detected at 10x gain. Recorded signals were butterworth filtered (low-pass at 40Hz) and calcium signals (in z-score) were extracted using Doric neuroscience studio V6 (Doric Lenses). Signals were further down sampled to 60 Hz using Matlab (R2020b) signal analyzer to match the behavioral sampling data (60 fps). Z-score > 2.56 (alpha = 0.01) was determined to be a calcium event. For heat map of cumulative time and calcium events, spatial binning was 50 pixels. To make correlation map (**Fig. S7 and S8a**), correlations between column of cumulative time heat map and cumulative calcium event heat map were tested using Matlab corr function.

Statistical analysis

Data and statistical analysis were performed with MATLAB R2020b (Mathworks). Unless otherwise noted, group data was presented as median, and first and third quartiles are shown for dispersion. Statistics were performed using a non-parametric test (signed-rank test for paired data and rank-sum test for unpaired data). One-way ANOVA (post hoc test: Tukey-Kramer test or Kruskal-Wallis test) were applied for multi-group comparison. Two-way ANOVA were performed for comparison of multi-factors. Pearson correlation coefficient was applied for correlation analysis. Significance was defined as $*p < 0.05$, $**p < 0.01$, $***p < 0.001$. Outlier was detected by Grubbe test (GraphPad, significant level: 0.05). Sample number were indicated as "n", animal number were indicated as "N".

References

1 Narikiyo, K. *et al.* The claustrum coordinates cortical slow-wave activity. *Nat Neurosci* **23**, 741-753 (2020). https://doi.org:10.1038/s41593-020-0625-7

2 Norimoto, H. *et al.* A claustrum in reptiles and its role in slow-wave sleep. *Nature* **578**, 413-418 (2020). https://doi.org:10.1038/s41586-020-1993-6

3 Crick, F. C. & Koch, C. What is the function of the claustrum? *Philos Trans R Soc Lond B Biol Sci* **360**, 1271-1279 (2005). https://doi.org:10.1098/rstb.2005.1661

4 Smith, J. B., Lee, A. K. & Jackson, J. The claustrum. *Curr Biol* **30**, R1401-R1406 (2020). https://doi.org:10.1016/j.cub.2020.09.069

5 Goll, Y., Atlan, G. & Citri, A. Attention: the claustrum. *Trends Neurosci* **38**, 486-495 (2015). https://doi.org:10.1016/j.tins.2015.05.006

6 Gardiner, J. M. & Parkin, A. J. Attention and recollective experience in recognition memory. *Mem Cognit* **18**, 579-583 (1990). https://doi.org:10.3758/bf03197100

7 Siegel, A. L. M. & Castel, A. D. The role of attention in remembering important item-location associations. *Mem Cognit* **46**, 1248-1262 (2018). https://doi.org:10.3758/s13421-018-0834-4

8 Chen, C. Y. *et al.* The cognitive dysfunction of claustrum on Alzheimer's disease: A mini-review. *Front Aging Neurosci* **15**, 1109256 (2023). https://doi.org:10.3389/fnagi.2023.1109256

9 Cascella, N. G., Gerner, G. J., Fieldstone, S. C., Sawa, A. & Schretlen, D. J. The insula-claustrum region and delusions in schizophrenia. *Schizophr Res* **133**, 77-81 (2011). https://doi.org:10.1016/j.schres.2011.08.004

10 Wang, X., Jiao, Y., Tang, T., Wang, H. & Lu, Z. Altered regional homogeneity patterns in adults with attention-deficit hyperactivity disorder. *Eur J Radiol* **82**, 1552-1557 (2013). https://doi.org:10.1016/j.ejrad.2013.04.009

11 Smith, J. B. *et al.* The relationship between the claustrum and endopiriform nucleus: A perspective towards consensus on cross-species homology. *J Comp Neurol* **527**, 476-499 (2019). https://doi.org:10.1002/cne.24537

12 Grimstvedt, J. S. *et al.* A multifaceted architectural framework of the mouse claustrum complex. *J Comp Neurol* **531**, 1772-1795 (2023). https://doi.org:10.1002/cne.25539

13 Behan, M. & Haberly, L. B. Intrinsic and efferent connections of the endopiriform nucleus in rat. *J Comp Neurol* **408**, 532-548 (1999).

14 Majak, K. & Morys, J. Endopiriform nucleus connectivities: the implications for epileptogenesis and epilepsy. *Folia Morphol (Warsz)* **66**, 267-271 (2007).

15 Fu, W., Sugai, T., Yoshimura, H. & Onoda, N. Convergence of olfactory and gustatory connections onto the endopiriform nucleus in the rat. *Neuroscience* **126**, 1033-1041 (2004). https://doi.org:10.1016/j.neuroscience.2004.03.041

16 Watson, G. D. R., Smith, J. B. & Alloway, K. D. Interhemispheric connections between the infralimbic and entorhinal cortices: The endopiriform nucleus has limbic connections that parallel the sensory and motor connections of the claustrum. *J Comp Neurol* **525**, 1363-1380 (2017). https://doi.org:10.1002/cne.23981

17 Pi, G. *et al.* Posterior basolateral amygdala to ventral hippocampal CA1 drives approach behaviour to exert an anxiolytic effect. *Nat Commun* **11**, 183 (2020). https://doi.org:10.1038/s41467-019-13919-3

18 Ciocchi, S., Passecker, J., Malagon-Vina, H., Mikus, N. & Klausberger, T. Brain computation. Selective information routing by ventral hippocampal CA1 projection neurons. *Science* **348**, 560-563 (2015). https://doi.org:10.1126/science.aaa3245

19 Hunsaker, M. R., Fieldsted, P. M., Rosenberg, J. S. & Kesner, R. P. Dissociating the roles of dorsal and ventral CA1 for the temporal processing of spatial locations, visual objects, and odors. *Behav Neurosci* **122**, 643-650 (2008). https://doi.org:10.1037/0735-7044.122.3.643

20 Okuyama, T., Kitamura, T., Roy, D. S., Itohara, S. & Tonegawa, S. Ventral CA1 neurons store social memory. *Science* **353**, 1536-1541 (2016). https://doi.org:10.1126/science.aaf7003

21 Kesner, R. P., Hunsaker, M. R. & Ziegler, W. The role of the dorsal and ventral hippocampus in olfactory working memory. *Neurobiol Learn Mem* **96**, 361-366 (2011). https://doi.org:10.1016/j.nlm.2011.06.011

547 22 Meira, T. *et al.* A hippocampal circuit linking dorsal CA2 to ventral CA1 critical for social
548 memory dynamics. *Nat Commun* **9**, 4163 (2018). https://doi.org:10.1038/s41467-018-
549 06501-w
550 23 Tanimizu, T. *et al.* Functional Connectivity of Multiple Brain Regions Required for the
551 Consolidation of Social Recognition Memory. *J Neurosci* **37**, 4103-4116 (2017).
552 https://doi.org:10.1523/JNEUROSCI.3451-16.2017
553 24 Tao, S. *et al.* Whole-Brain Mapping the Direct Inputs of Dorsal and Ventral CA1 Projection
554 Neurons. *Front Neural Circuits* **15**, 643230 (2021). https://doi.org:10.3389/fncir.2021.643230
555 25 Gergues, M. M. *et al.* Circuit and molecular architecture of a ventral hippocampal network.
556 *Nat Neurosci* **23**, 1444-1452 (2020). https://doi.org:10.1038/s41593-020-0705-8
557 26 Kitanishi, T. & Matsuo, N. Organization of the Claustrum-to-Entorhinal Cortical Connection in
558 Mice. *J Neurosci* **37**, 269-280 (2017). https://doi.org:10.1523/JNEUROSCI.1360-16.2016
559 27 Qadir, H. *et al.* Structural Connectivity of the Anterior Cingulate Cortex, Claustrum, and the
560 Anterior Insula of the Mouse. *Front Neuroanat* **12**, 100 (2018).
561 https://doi.org:10.3389/fnana.2018.00100
562 28 Jackson, J., Karnani, M. M., Zemelman, B. V., Burdakov, D. & Lee, A. K. Inhibitory Control of
563 Prefrontal Cortex by the Claustrum. *Neuron* **99**, 1029-1039 e1024 (2018).
564 https://doi.org:10.1016/j.neuron.2018.07.031
565 29 Smith, J. B. & Alloway, K. D. Functional specificity of claustrum connections in the rat:
566 interhemispheric communication between specific parts of motor cortex. *J Neurosci* **30**,
567 16832-16844 (2010). https://doi.org:10.1523/JNEUROSCI.4438-10.2010
568 30 Pelkey, K. A. *et al.* Hippocampal GABAergic Inhibitory Interneurons. *Physiol Rev* **97**, 1619-
569 1747 (2017). https://doi.org:10.1152/physrev.00007.2017
570 31 Song, J. H. *et al.* Precise Mapping of Single Neurons by Calibrated 3D Reconstruction of Brain
571 Slices Reveals Topographic Projection in Mouse Visual Cortex. *Cell Rep* **31**, 107682 (2020).
572 https://doi.org:10.1016/j.celrep.2020.107682
573 32 Freund, T. F. & Antal, M. GABA-containing neurons in the septum control inhibitory
574 interneurons in the hippocampus. *Nature* **336**, 170-173 (1988).
575 https://doi.org:10.1038/336170a0
576 33 Bilash, O. M., Chavlis, S., Johnson, C. D., Poirazi, P. & Basu, J. Lateral entorhinal cortex inputs
577 modulate hippocampal dendritic excitability by recruiting a local disinhibitory microcircuit.
578 *Cell Rep* **42**, 111962 (2023). https://doi.org:10.1016/j.celrep.2022.111962
579 34 Petreanu, L., Mao, T., Sternson, S. M. & Svoboda, K. The subcellular organization of
580 neocortical excitatory connections. *Nature* **457**, 1142-1145 (2009).
581 https://doi.org:10.1038/nature07709
582 35 Danielson, N. B. *et al.* Sublayer-Specific Coding Dynamics during Spatial Navigation and
583 Learning in Hippocampal Area CA1. *Neuron* **91**, 652-665 (2016).
584 https://doi.org:10.1016/j.neuron.2016.06.020
585 36 Mathis, A. *et al.* DeepLabCut: markerless pose estimation of user-defined body parts with
586 deep learning. *Nat Neurosci* **21**, 1281-1289 (2018). https://doi.org:10.1038/s41593-018-
587 0209-y
588 37 Lauer, J. *et al.* Multi-animal pose estimation, identification and tracking with DeepLabCut.
589 *Nat Methods* **19**, 496-504 (2022). https://doi.org:10.1038/s41592-022-01443-0
590 38 Roth, B. L. DREADDs for Neuroscientists. *Neuron* **89**, 683-694 (2016).
591 https://doi.org:10.1016/j.neuron.2016.01.040
592 39 Jimenez, J. C. *et al.* Anxiety Cells in a Hippocampal-Hypothalamic Circuit. *Neuron* **97**, 670-683
593 e676 (2018). https://doi.org:10.1016/j.neuron.2018.01.016
594 40 Jimenez, J. C. *et al.* Contextual fear memory retrieval by correlated ensembles of ventral CA1
595 neurons. *Nat Commun* **11**, 3492 (2020). https://doi.org:10.1038/s41467-020-17270-w
596 41 Bekkers, J. M. & Suzuki, N. Neurons and circuits for odor processing in the piriform cortex.
597 *Trends Neurosci* **36**, 429-438 (2013). https://doi.org:10.1016/j.tins.2013.04.005

42 Feinberg, L. M., Allen, T. A., Ly, D. & Fortin, N. J. Recognition memory for social and non-social odors: differential effects of neurotoxic lesions to the hippocampus and perirhinal cortex. *Neurobiol Learn Mem* **97**, 7-16 (2012). https://doi.org:10.1016/j.nlm.2011.08.008

43 Shu, Y., Hasenstaub, A. & McCormick, D. A. Turning on and off recurrent balanced cortical activity. *Nature* **423**, 288-293 (2003). https://doi.org:10.1038/nature01616

44 Li, X. G., Somogyi, P., Tepper, J. M. & Buzsaki, G. Axonal and dendritic arborization of an intracellularly labeled chandelier cell in the CA1 region of rat hippocampus. *Exp Brain Res* **90**, 519-525 (1992). https://doi.org:10.1007/BF00230934

45 Klausberger, T. & Somogyi, P. Neuronal diversity and temporal dynamics: the unity of hippocampal circuit operations. *Science* **321**, 53-57 (2008). https://doi.org:10.1126/science.1149381

46 Dudok, B. *et al.* Recruitment and inhibitory action of hippocampal axo-axonic cells during behavior. *Neuron* **109**, 3838-3850 e3838 (2021). https://doi.org:10.1016/j.neuron.2021.09.033

47 Chiang, M. C., Huang, A. J. Y., Wintzer, M. E., Ohshima, T. & McHugh, T. J. A role for CA3 in social recognition memory. *Behav Brain Res* **354**, 22-30 (2018). https://doi.org:10.1016/j.bbr.2018.01.019

48 Tao, K. *et al.* Disrupted social memory ensembles in the ventral hippocampus underlie social amnesia in autism-associated Shank3 mutant mice. *Mol Psychiatry* **27**, 2095-2105 (2022). https://doi.org:10.1038/s41380-021-01430-5

49 Deng, X., Gu, L., Sui, N., Guo, J. & Liang, J. Parvalbumin interneuron in the ventral hippocampus functions as a discriminator in social memory. *Proc Natl Acad Sci U S A* **116**, 16583-16592 (2019). https://doi.org:10.1073/pnas.1819133116

50 Wei, J. A. *et al.* Amygdala neural ensemble mediates mouse social investigation behaviors. *Natl Sci Rev* **10**, nwac179 (2023). https://doi.org:10.1093/nsr/nwac179

51 Franklin, T. B. *et al.* Prefrontal cortical control of a brainstem social behavior circuit. *Nat Neurosci* **20**, 260-270 (2017). https://doi.org:10.1038/nn.4470

52 Shah, A. A. & Treit, D. Excitotoxic lesions of the medial prefrontal cortex attenuate fear responses in the elevated-plus maze, social interaction and shock probe burying tests. *Brain Res* **969**, 183-194 (2003). https://doi.org:10.1016/s0006-8993(03)02299-6

53 Puchades, M. A., Csucs, G., Ledergerber, D., Leergaard, T. B. & Bjaalie, J. G. Spatial registration of serial microscopic brain images to three-dimensional reference atlases with the QuickNII tool. *PLoS One* **14**, e0216796 (2019). https://doi.org:10.1371/journal.pone.0216796

54 Mesic, I. *et al.* Double Dissociation of the Roles of Metabotropic Glutamate Receptor 5 and Oxytocin Receptor in Discrete Social Behaviors. *Neuropsychopharmacology* **40**, 2337-2346 (2015). https://doi.org:10.1038/npp.2015.81

55 Rein, B., Ma, K. & Yan, Z. A standardized social preference protocol for measuring social deficits in mouse models of autism. *Nat Protoc* **15**, 3464-3477 (2020). https://doi.org:10.1038/s41596-020-0382-9

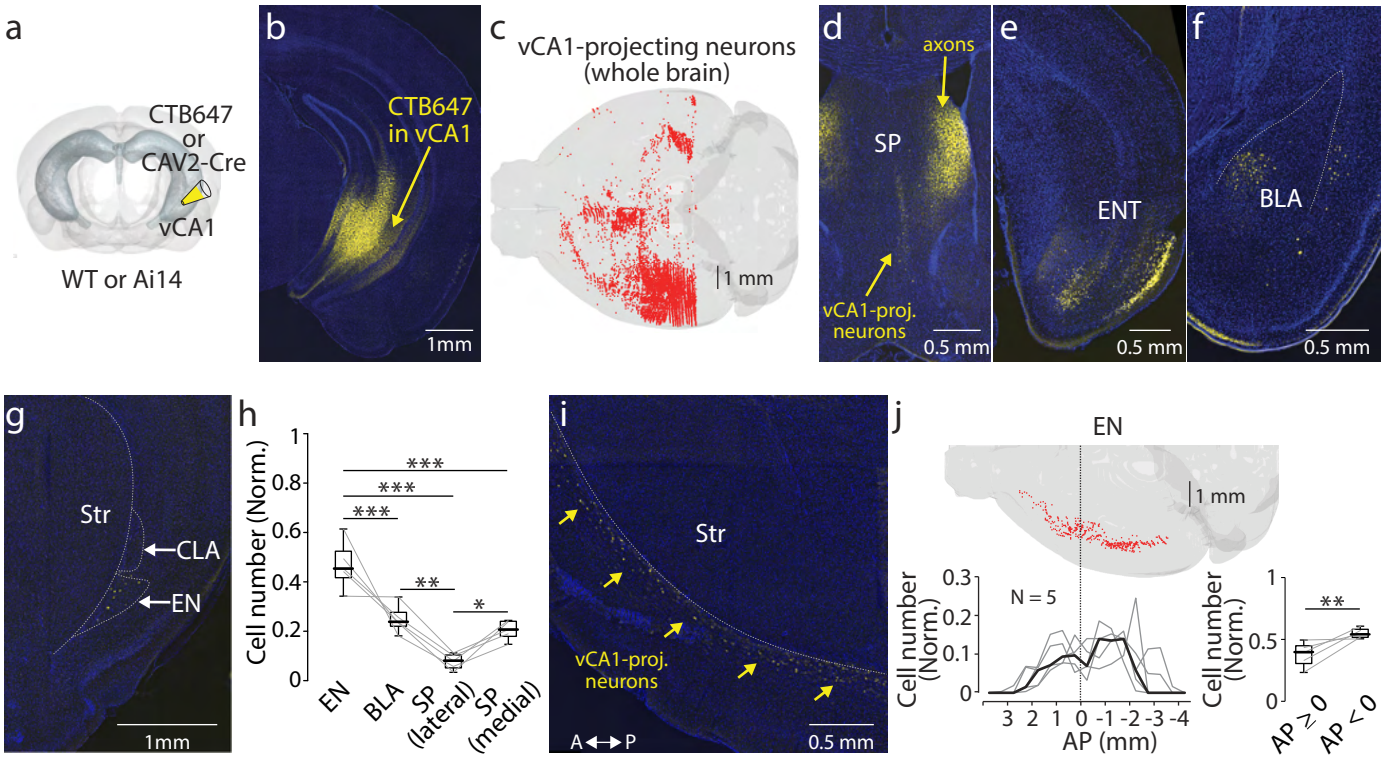

Figure 1. Endopiriform projects to the ventral CA1

(**a**) Schematic diagram of a retrograde tracer injection performed. CAV-2-Cre or CTB647 was used in combination with Ai14 or wild-type mice, respectively. (**b**) An example fluorescent image of injection site. (**c**) Distribution of retrogradely labeled vCA1-projecting neurons in entire brain as a result of injection in panel b. (**d-g**) Fluorescent images showing retrogradely labeled vCA1-projecitng neurons in septum (SP), entorhinal cortex (ENT), basolateral amygdala (BLA), and endopiriform (EN). Str: Striatum, CLA: Claustrum. (**h**) Box plots showing relative number of vCA1-projecting neurons in different brain areas. Cell numbers in each brain area were normalized by summed cell number of EN, BLA, SP (lateral), and SP (medial). Median value for EN, BLA, SP (lateral), and SP (medial) is 0.45, 0.24, 0.08, and 0.21, respectively. Statistics: EN vs BLA, SP (lateral), or SP (medial), $p < 0.001$ for all; BLA vs SP (lateral) or SP (medial): $p = 0.002$ and 0.694, respectively; SP (lateral) vs SP (medial) $p = 0.023$. One-way ANOVA, repeated comparison with Tukey-Kramer test. N = 5. (**i**) An example fluorescent image of horizontal section showing retrogradely labeled vCA1-projecting neurons in EN. A: anterior, P: posterior. (**j**) Top: Example map showing distribution of vCA1-projecting neurons in entire EN in one mouse. Bottom left: A plot showing a quantified distribution at bin size of 1 mm. Each bin was normalized to total number of labeled neurons in EN. Data from each mouse are shown in grey. Median is indicated in black. Bottom right: Box plots comparing a number of vCA1-projecting neurons in anterior and posterior EN. Data were normalized to a total number of labeled neurons in EN. Median value for anterior vs posterior is 0.39 vs 0.54. Statistics: $p = 0.008$, Rank-sum.

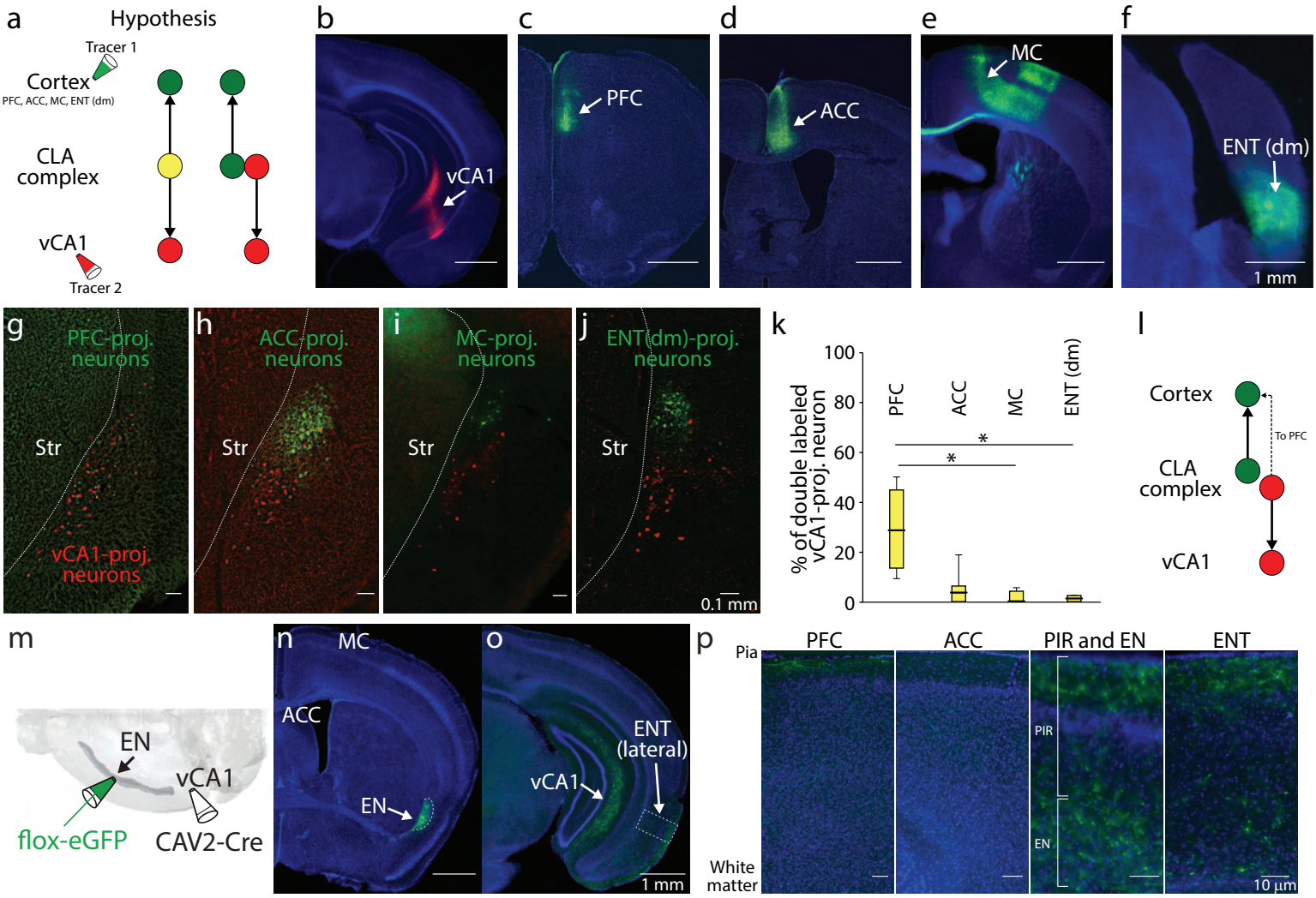

Figure 2. Axon branching of vCA1-projecting EN neurons

(**a**) Schematic diagram of injection performed and two hypothesized outcomes. Yellow color indicates double-labeled neurons. PFC: Prefrontal cortex, ACC: Anterior cingulate cortex, MC: Motor cortex, ENT(dm): Dorsomedial entorhinal cortex. (**b-f**) Example fluorescent images of injection site for each region indicated. (**g-j**) Example fluorescent images of retrogradely labeled neurons in CLA complex. vCA1-projecting neurons were colored in red and cortex-projecting neurons were colored in green. (**k**) Box plots showing percentage of double-labeled vCA1-projecting neurons for each cortical injection. Medial value for PFC, ACC, MC, and ENT(dm) was 28.6, 4.6, 0, and 1.2, respectively. Statistics: PFC vs MC or ENT(dm), p = 0.015 and 0.047, respectively. One-way ANOVA with post-hoc Kruskal-Wallis test. Slice and animal number: 16 and 4 for PFC, 20 and 5 for ACC, 10 and 3 for MC, and 18 and 4 for ENT(dm). (**l**) Schematic diagram of projection pattern found in the experiment shown in A. (**m**) Schematic diagram of the intersectional approach performed to label vCA1-projecting EN neurons.
(**n-o**) Example fluorescent images showing vCA1-projectig axons in different brain areas. All images were from the same mouse. (**p**) Magnified images showing vCA1-projecting axons in cortical layers. Magnified areas are indicated in **o** and fig. **S2a-c** as dashed squares. PIR: Piriform cortex

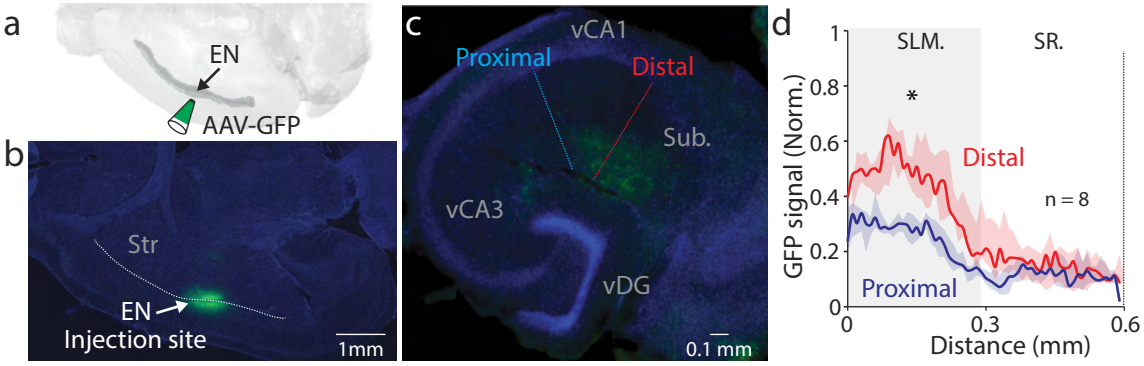

Figure 3. EN projection pattern in vCA1

(**a**) Schematic diagram of injection performed. (**b**) An example fluorescent image of horizontal brain section containing injection site in EN. (**c**) An example fluorescent image of ventral hippocampal slice with EN axons resulted from the injection in (**b**). Distal and proximal vCA1 where GFP signals were measured were indicated by dashed lines. (**d**) Normalized GFP signals across the layer. All signals were normalized by maximum GFP signal in the distal subregion. Median of area under the curve: distal; 11.12, proximal; 5.99. distal vs proximal, $p = 0.016$. Wilcoxon signed-rank test. $n = 8$ slices ($N = 4$ mice). SR: stratum radiatum, Py: pyramidal layer.

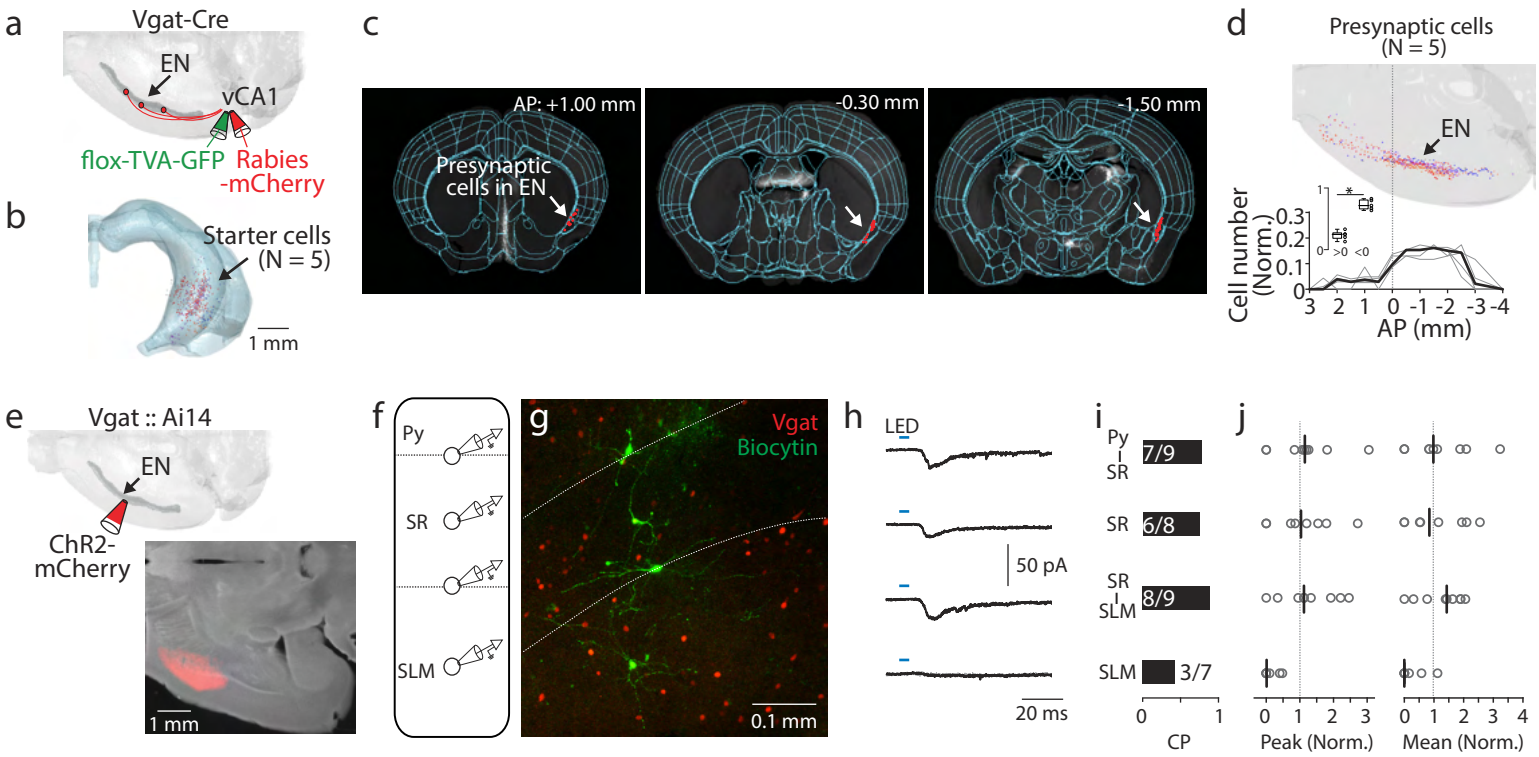

Figure 4. EN$^{vCA1\text{-}proj.}$ neurons target vCA1 interneurons

(**a**) Schematic diagram of injection performed for monosynaptic rabies tracing. (**b**) Location of starter cells in the hippocampus. Data from 5 brains were overlaid. (**c**) Example images showing presynaptic cells in EN (white arrow). (**d**) Top: Location of presynaptic EN neurons. Data from 5 brains were overlaid. Bottom: Plots indicate distribution of presynaptic cells in EN along AP axis. Cell counts in a given bin (1 mm) were normalized by total cell number in EN. Thin gray lines indicate individual data. A thick black line indicates median. Inset showing plot comparing cell number in anterior and posterior location as in Fig. 1j. Median: anterior vs posterior, 0.25 vs 0.72, p = 0.031; Wilcoxon signed-rank test. (**e**) Top: Schematic diagram of injection performed. Bottom: An example fluorescent image of injection site in EN. (**f**) Schematic diagram of recordings performed. Recordings were performed from identified GABAergic neurons sequentially in a random order. (**g**) An example confocal image of an acute vCA1 slice used for recordings. Recorded GABAergic neurons were filled with biocytin and post-labeled with Alexa488. White dashed lines indicate border of Py-SR and SR-SLM. (**h**) Median traces of photo-evoked EPSCs recorded from neurons at different laminar position. (**i**) Connection probability (CP) of EN axons and recorded neurons at different laminar positions. Numbers in bars indicate number of response positive neurons /total recorded neurons. (**j**) Left: Peak amplitudes of evoked EPSCs (normalized to total input from recorded slice). Right: the same as left but for mean amplitude. Gray circles indicate each neuron. Black lines indicate median. Median (peak amp): Py-SR vs SR vs SR-SLM vs SLM: 1.1 vs 1.0 vs 1.1 vs 0.0. [Py-SR,SR, SR/SLM vs SLM], p = 0.076, 0.111, 0.04; one-way ANOVA, repeated comparison with Tukey-Kramer test. Median (mean amp): Py-SR vs SR vs SR-SLM vs SLM: 1.0 vs 0.8 vs 1.4 vs 0.0. [Py-Sr, SR, SR-SLM vs SLM], p = 0.14, 0.251, and 0.114; one-way ANOVA, repeated comparison with Tukey-Kramer test. N = 5 mice.

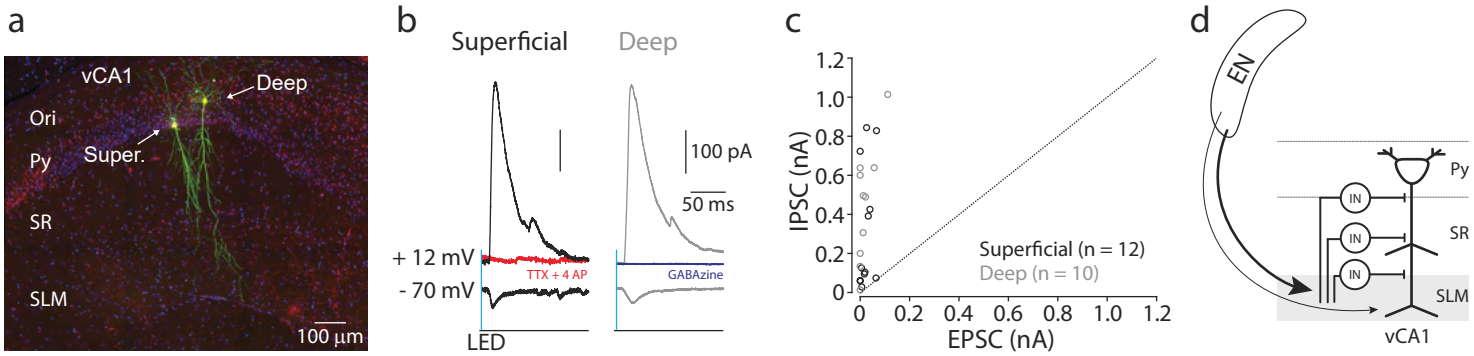

Figure 5. EN dsynaptically inhibits vCA1 pyramidal neurons

(**a**) A confocal image of recorded pyramidal neurons in vCA1. Recorded pyramidal neurons were filled with biocytin and post-labelled with Alexa488. Ori.: oriens, Super.: superficial layer pyramidal neuron. Deep: deep layer pyramidal neuron. (**b**) Example traces of photo-evoked EPSCs and IPSCs in superficial (black trace) and deep (gray trace) pyramidal neurons. Red trace: after TTX and 4AP. Blue trace: after gabazine. (**c**) Scatter plots of peak amplitudes of EPSCs and IPSCs for each neuron. Dashed line indicates a unitary line. Superficial neurons: empty Black circles. Deep neurons: Gray circles. N = 4 mice. (**d**) A summary diagram of EN-vCA1 circuit. In vCA1, EN axons innervate GABAergic neurons (IN), which in turn inhibits pyramidal neurons (both superficial and deep).

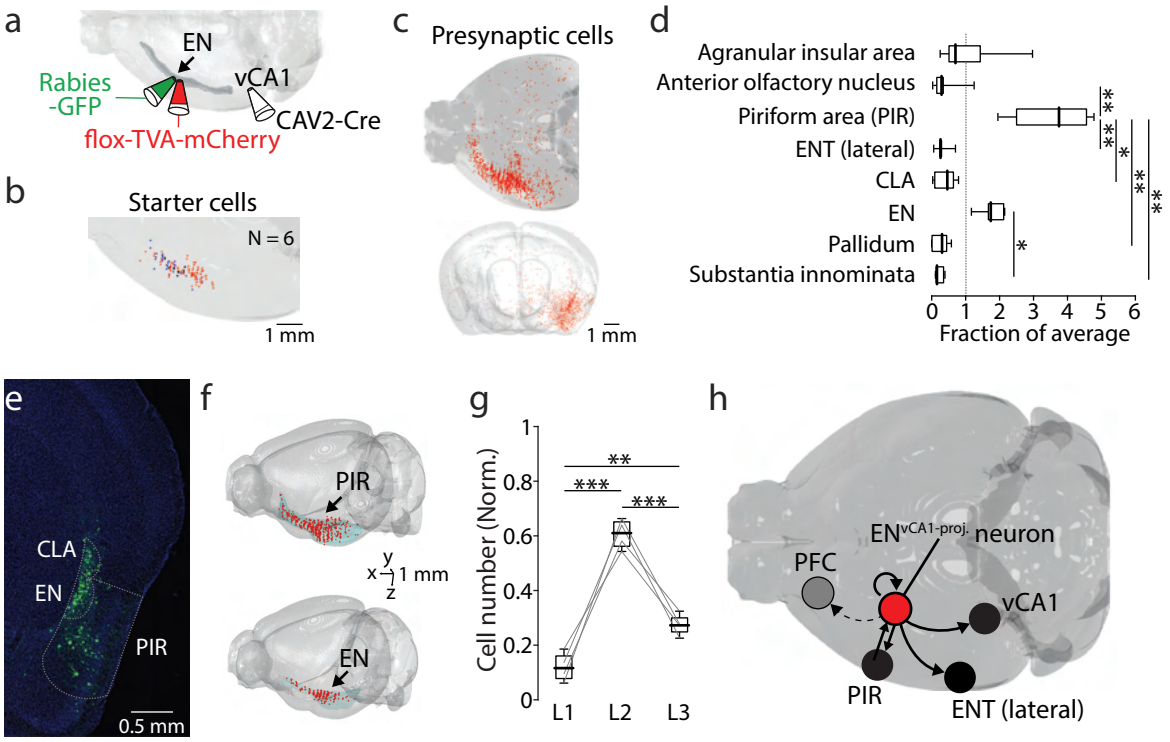

Figure 6. EN$^{vCA1\text{-}proj.}$ neurons receive inputs from the piriform cortex and within EN

(**a**) Schematic diagram of performed. (**b**) Location of starter cells in EN. Data from 6 brains were overlaid. (**c**) An example map of presynaptic cells in one brain. Top: Horizontal view. Injections were made in left hemisphere. Bottom: Front view. (**d**) Number of presynaptic cells in different brain areas (normalized to total presynaptic cell number). Median for AIA, AON, PIR, ENT(lateral), CLA, EN, Pallidum, and SI (in fraction): 0.7, 0.3, 3.8, 0.3, 0.5, 1.7, 0.3, and 0.2. [AON, ENT(lateral), CLA, Pallidum, SI] vs PIR: $p = 0.016$, 0.008, 0.048, 0.006, and 0.003. EN vs SI, $p = 0.043$. one-way ANOVA with post-hoc Kruskal-Wallis test. Full list of statistical tests and p values are in supplemental table. (**e**) An example fluorescent image of coronal slice containing EN and PIR and labeled presynaptic cells. (**f**) Example maps of presynaptic cells in PIR (top) and EN (bottom). (**g**) Number of presynaptic cells in PIR in different layers (normalized to the total number of labeled neurons in PIR). Median: L1 vs L2 vs L3, 0.11 vs 0.61 vs 0.27. L1 vs L2, $p < 0.001$; L1 vs L3, $p = 0.005$; L2 vs L3, $p < 0.001$; one-way ANOVA, repeated comparison with Tukey-Kramer test. (**h**) Summary diagram showing input-output circuit of EN$^{vCA1\text{-}proj.}$ neurons (red circle).

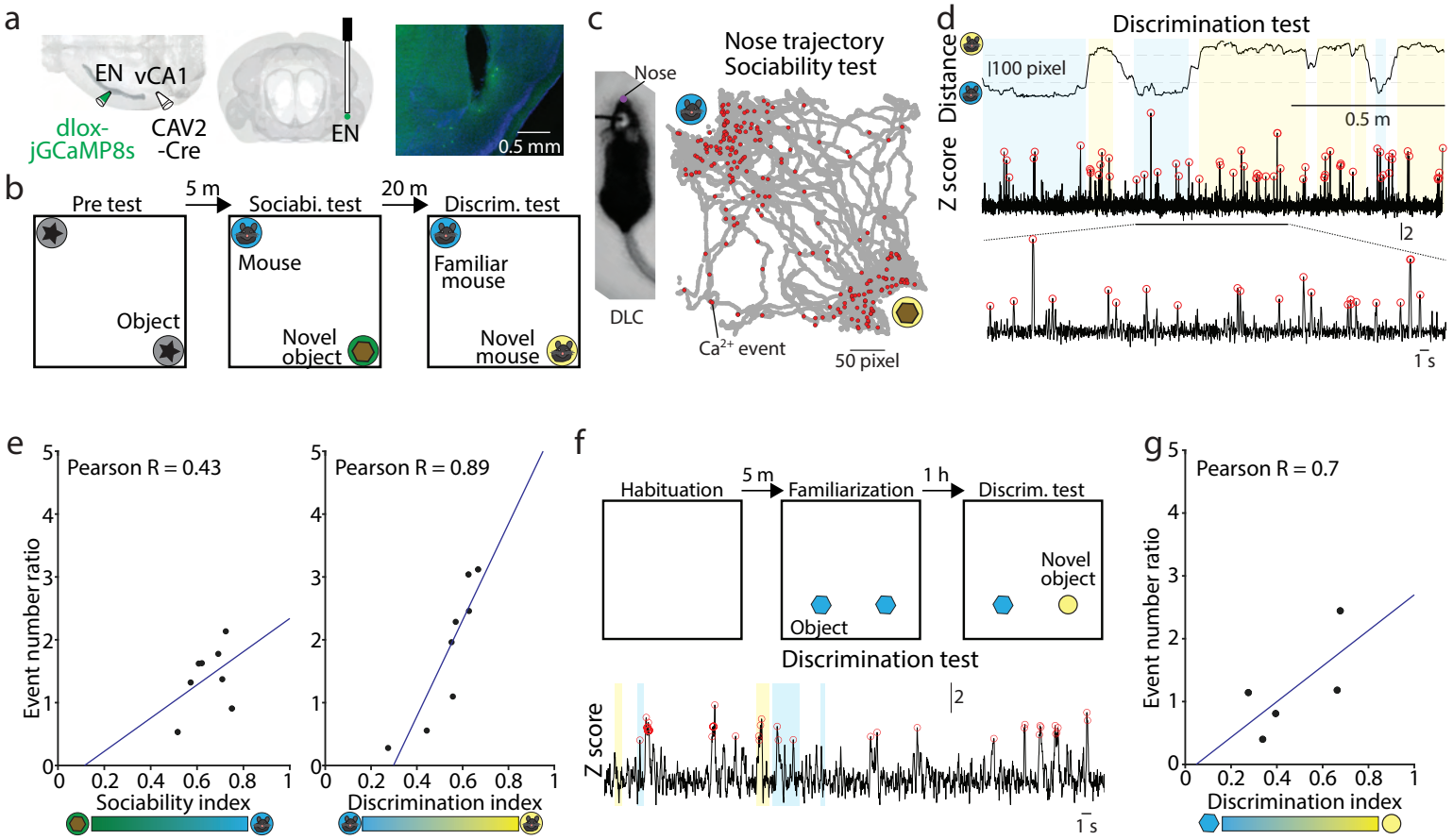

Figure 7. Activity of EN$^{vCA1\text{-}proj.}$ neurons predict social/object discrimination performance

(**a**) Right and Middle: Schematic diagram of injection and optic cannula implantation performed. Left: An example image showing jGCaMP8s expressing EN$^{vCA1\text{-}proj.}$ neurons and a tract of optic cannula. (**b**) The diagram of social recognition memory test. A test consisted of pretest (5 min), sociability test (10 min), and discrimination test (5 min). (**c**) Left: An example image of a mouse with nose point marker tracked by DLC. Right: An example map of nose points and calcium events in the arena during sociability test. **(d)** Nose distance vector (distance between subject's nose point and a center point of novel/familiar mouse chambers) and simultaneously acquired calcium signals during discrimination test. Gray dashed lines indicate the border of interaction zones. Open red circles indicate the calcium event detected (threshold: $Z > 2.58$). A part of calcium signal trace was expanded at the bottom for clarity. (**e**) Left: Correlation between calcium event ratios (calcium event number in the mouse interaction zone/ calcium event number in the object interaction zone) and sociability index. $p = 0.29$, $N = 8$ mice. Right: same as in left panel, but for calcium event ratios (calcium event number in the unfamiliar mouse interaction zone/ calcium event number in the familiar mouse interaction zone) and discrimination index. $p = 0.003$, $N = 8$. (**f**) The diagram of novel object recognition memory test. A test consisted of habituation (5 min), familiarization (10 min), and discrimination test (5 min). (**g**) Same as in (**e**), but for calcium event number ratios (calcium event number in the unfamiliar object interaction zone/calcium event number in the familiar object interaction zone and discrimination index. $p = 0.193$. $N = 5$ mice.

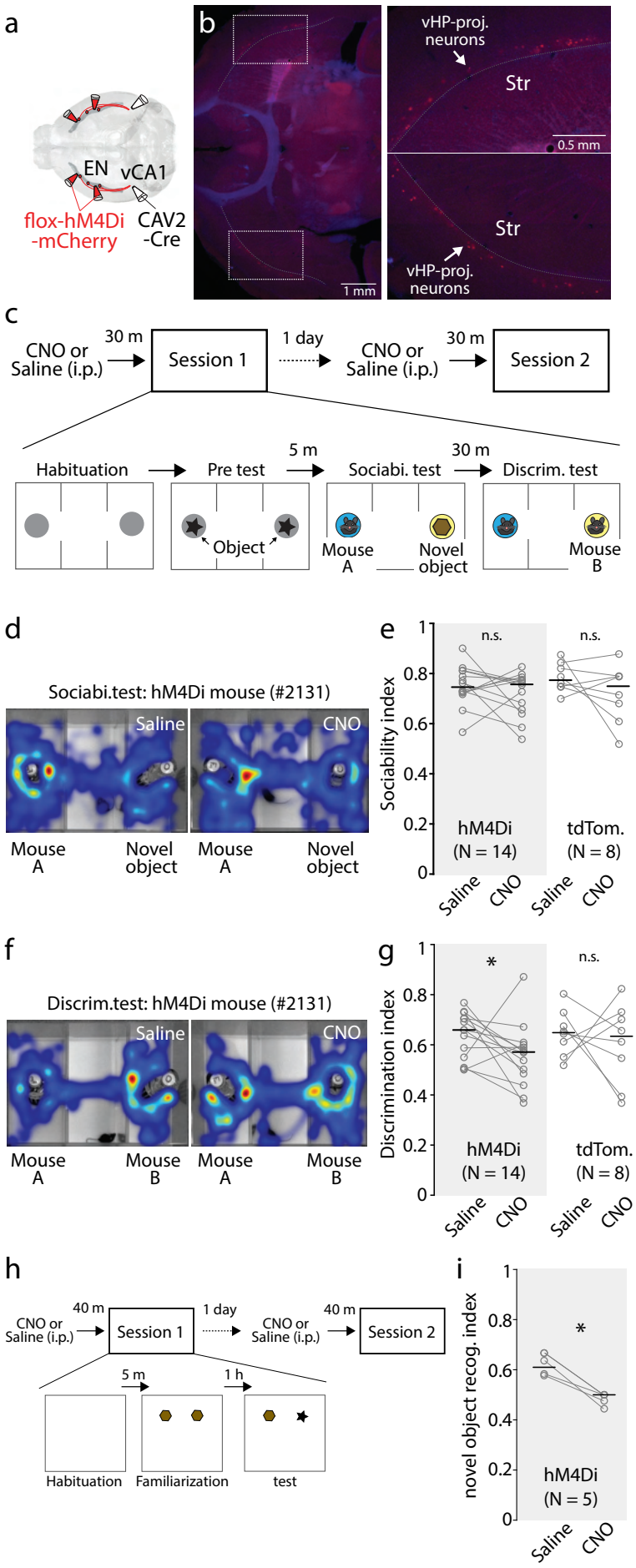
a
EN
vCA1
flox-hM4Di
-mCherry
CAV2
-Cre
b
1 mm
vHP-proj.
neurons
Str
0.5 mm
Str
vHP-proj.
neurons
c
CNO or
Saline (i.p.)
30 m
Session 1
1 day
CNO or
Saline (i.p.)
30 m
Session 2
Habituation
Pre test
5 m
Sociabi. test
30 m
Discrim. test
Object
Mouse
A
Novel
object
Mouse
B
d
Sociabi.test: hM4Di mouse (#2131)
Saline
CNO
Mouse
A
Novel
object
Mouse
A
Novel
object
e
Sociability index
n.s.
n.s.
hM4Di
(N = 14)
tdTom.
(N = 8)
Saline
CNO
Saline
CNO
f
Discrim.test: hM4Di mouse (#2131)
Saline
CNO
Mouse
A
Mouse
B
Mouse
A
Mouse
B
g
Discrimination index
*
n.s.
hM4Di
(N = 14)
tdTom.
(N = 8)
Saline
CNO
Saline
CNO
h
CNO or
Saline (i.p.)
40 m
Session 1
1 day
CNO or
Saline (i.p.)
40 m
Session 2
5 m
1 h
Habituation
Familiarization
test
i
novel object recog. index
*
hM4Di
(N = 5)
Saline
CNO

Figure 8. Chemogenetic inhibition of $EN^{vCA1\text{-}proj.}$ neurons specifically impairs recognition memory

(**a**) Schematic diagram of injection performed. (**b**) Left: An example fluorescent image showing expression of hM4Di in $EN^{CA1\text{-}proj.}$ neurons. Right: Expansion of areas marked by white rectangle in image on the left. (**c**) The diagram of social recognition memory test. A session consisted of habituation (5 min), Pretest (5 min), Sociability test (10 min), and discrimination test (5 min). The group treated with a saline in session 1 was treated with CNO (1mg/ kg) in session 2 the following day. (**d**) Example cumulative times heat map in arena during sociability tests for the same mouse under two different treatments. **(e)** Plots comparing sociability index for hM4Di and tdTomato mice under two different treatments. Gray empty circles indicate each mouse. Gray thin lines show paired data from one mouse. Thick black bars indicate median. Median sociability index: hM4Di mice (Saline vs CNO), 0.75 vs 0.76, $p = 0.391$; signed-rank test; tdTomato mice (Saline vs CNO), 0.77 vs 0.75, $p = 0.383$; signed-rank test. (**f**) Example cumulative time heat maps in arena during discrimination tests for the same mouse under two different treatments. (**g**) Comparison of discrimination index for hM4Di and tdTomato mice under two different treatments. Gray empty circles indicate each mouse. Gray thin lines show paired data from one mouse. Thick black bars indicate median. Median discrimination index: hM4Di mice (Saline vs CNO), 0.66 vs 0.57, $p = 0.042$; signed-rank test; tdTomato mice (Saline vs CNO), 0.65 vs 0.63, $p = 0.742$; signed-rank test. (**h**) The diagram of novel object recognition memory test. A session consists of habituation (5 min), familiarization (10 min), and discrimination test (5 min). CNO treatment was the same as in **c**. (**i**) Same as in **g**, but for novel object discrimination index. Median discrimination index: hM4Di mice (Saline vs CNO), 0.64 vs 0.5, $p = 0.003$; signed-rank test.

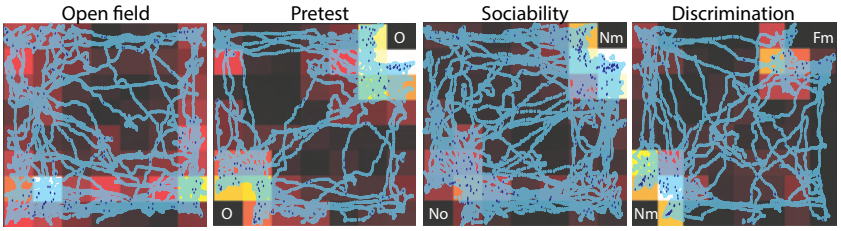

	Preference		
Conspecific Object	N.object N.object	N.object N.object	N.object N.mouse	N.mouse F.mouse N.object F.object
Ca^{2+} event	<	=	>
Time	<	<	>
GiDREADD	No change	No change	Impaired

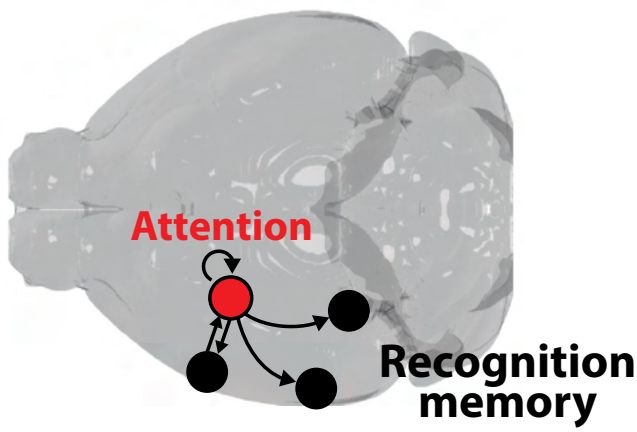

Figure.9 Summary of $EN^{vCA1\text{-}proj.}$ neurons circuits and their function proposed

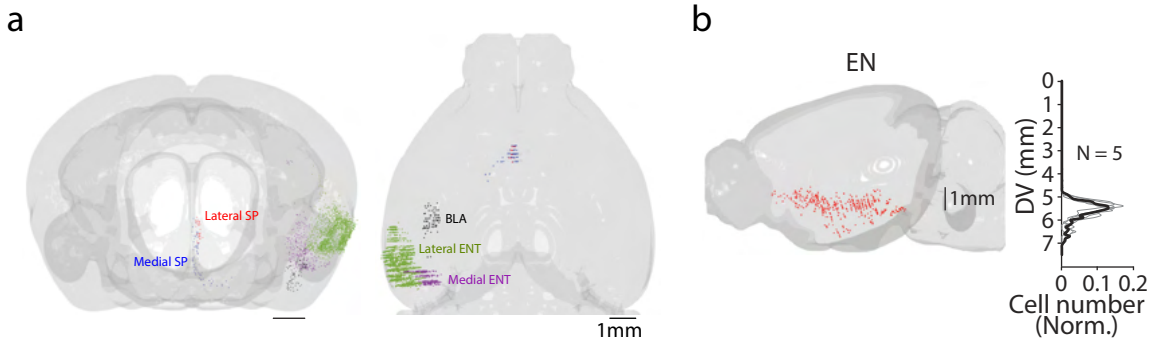

Figure S1. Related to figure 1.

(**a**) An example distribution map of vCA1-projecting neurons in SP (lateral and medial), BLA and ENT (lateral and medial) shown from front and top view. Neurons in different brain areas are color-coded. (**b**) The side view of the brain shown in **Fig.1j**. Plots indicate distribution of vCA1-projecting neurons in EN along dorsal-ventral axis (DV). Data from different mice are shown in gray. Median is indicated in black.

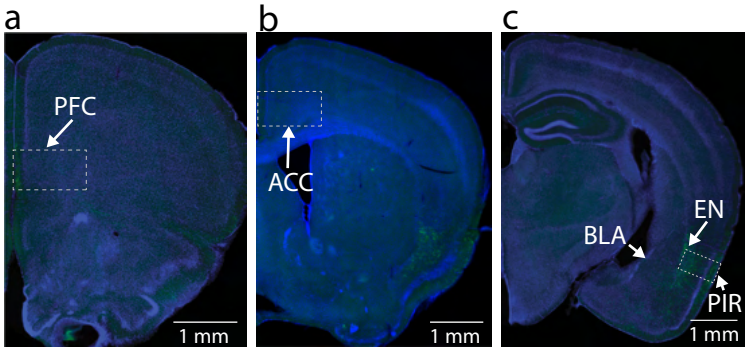

Figure S2. Related to figure 2.

(**a-c**) Example fluorescent images of branching of vCA1-projecting neurons. All images were from the same mouse shown in **Fig. 2n-o**.

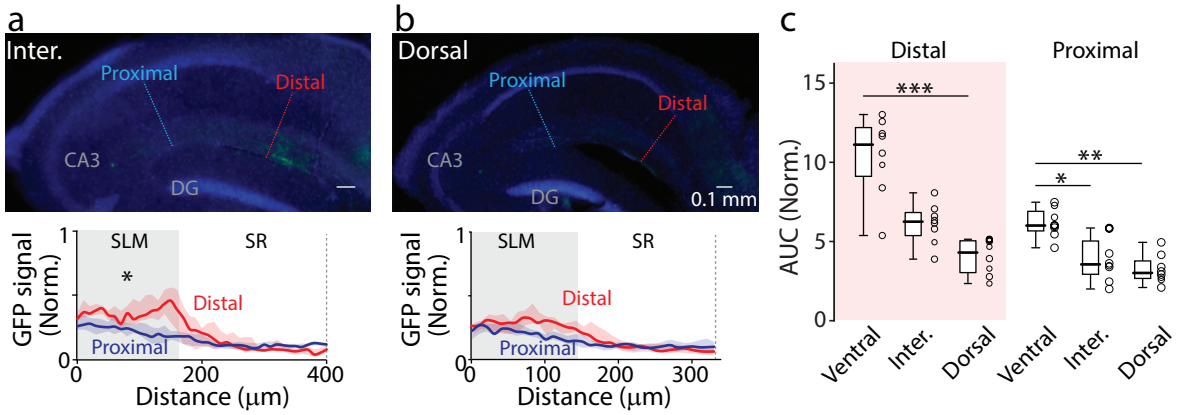

Figure S3. Related to figure 3.

(**a**) Top: An example fluorescent image of intermediate hippocampal sections from the same brain as in **Fig. 3b and c** Bottom: GFP signal profile at the distal and proximal region indicated in an image at the top. (**b**) The same as in (**a**) but for dorsal hippocampus. Median area under the curve (AUC): distal vs proximal (intermediate), 6.3 vs 3.5, $p = 0.007$; distal vs proximal (dorsal), 4.3 vs 3.0, $p = 0.055$; Wilcoxon signed-rank test. n = 8 slices (N = 4 mice). (**c**) Comparison of GFP signal (in AUC) between different hippocampal axis for distal or proximal vCA1. Distal; ventral vs intermediate, $p = 0.086$; ventral vs dorsal, $p < 0.001$; intermediate vs dorsal, $p = 0.136$. Proximal; ventral vs intermediate, $p = 0.018$; ventral vs dorsal, $p = 0.001$; intermediate vs dorsal, $p = 0.695$; Kruskal-Wallis test. n = 8 slices (N = 4 mice).

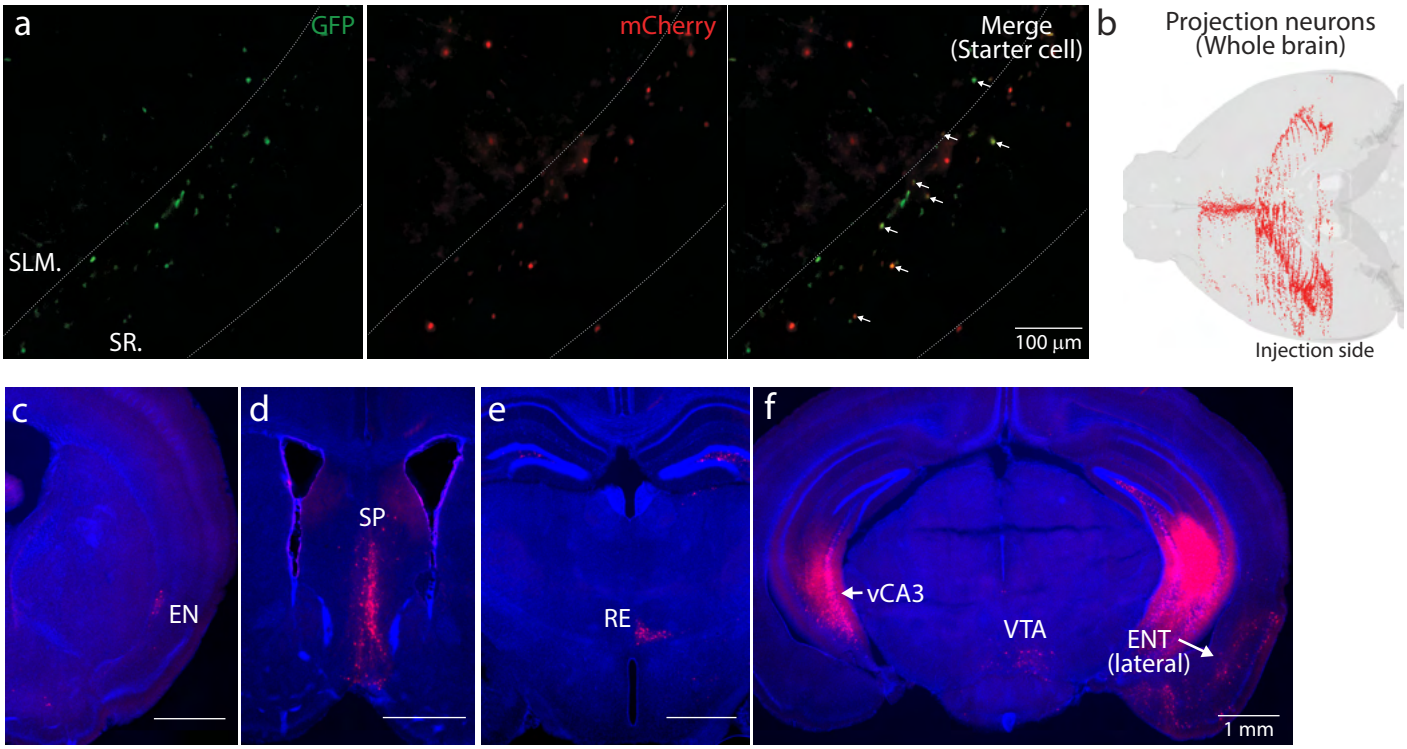

Figure S4. Related to figure 4.

(**a**) Example fluorescent images of starter cells in vCA1. TVA_oG expressing neurons were labeled by GFP and rabies expressing neurons were labeled by mCherry. GFP and mCherry double expressing neurons were counted as starter cells. White allows in right panel indicate starter cells. White dashed lines indicate the Py-SR and SR-SLM border. (**b**) An example map of presynaptic cells in a whole brain. Injection was made in the left hemisphere. (**c-f**) Fluorescent images of presynaptic cells in coronal sections from the same mouse brain. Presynaptic neurons were in EN (**c**), septum (SP) (**d**), nucleus reunion (RE) (**e**), contralateral vCA3 (vCA3) (**f**), ventral tegmental area (VTA) (**f**), and lateral ENT (**f**).

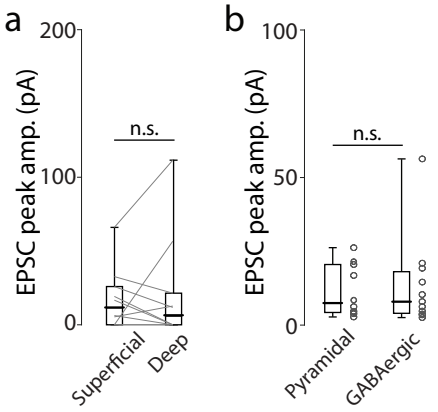

Figure S5. Related to figure 5.

(a) Plots comparing peak amplitude of photo-evoked EPSCs in superficial and deep pyramidal neurons. Thin gray lines indicate paired data. Median peak amplitude; superficial vs deep (in pA): 11.5 vs 5.9, p = 0.625; signed-rank test. **(b)** Plots comparing peak amplitude of photo-evoked EPSCs in pyramidal and GABAergic neurons. The data from superficial and deep pyramidal neurons were pooled. n = 10 for pyramidal neurons and 11 for GABAergic neurons. N = 4 mice. Median EPSC peak amplitude: Pyramidal vs GABAergic (in pA): 7.4 vs 8.0. p = 0.86. Rank-sum.

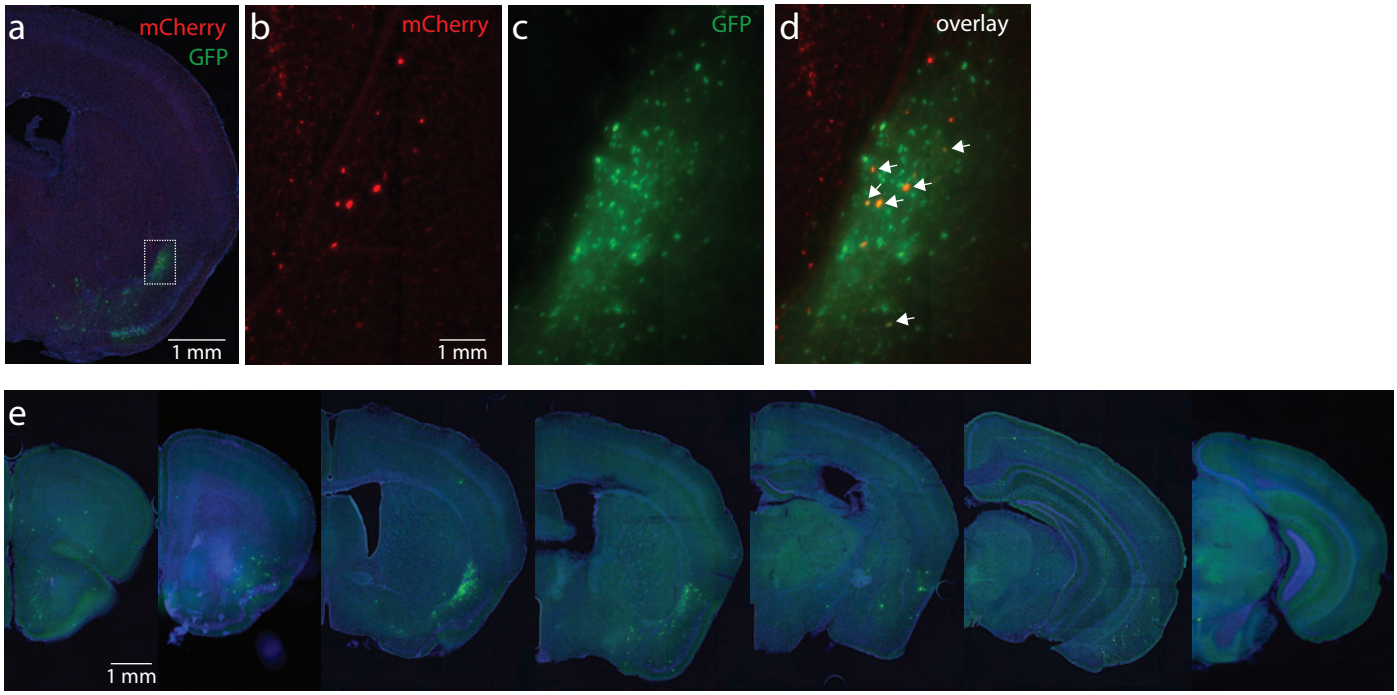

Figure S6. Related to figure 6.

(**a**) An example fluorescent image of starter cells in EN. (**b-d**) Expanded images of the area marked by white square in panel **a**. White allows indicate starter cells. (**e**) Example fluorescent images of coronal sections in series. Labeled neurons (in green) indicate presynaptic cells of EN $^{vCA1\text{-}proj.}$ neurons.

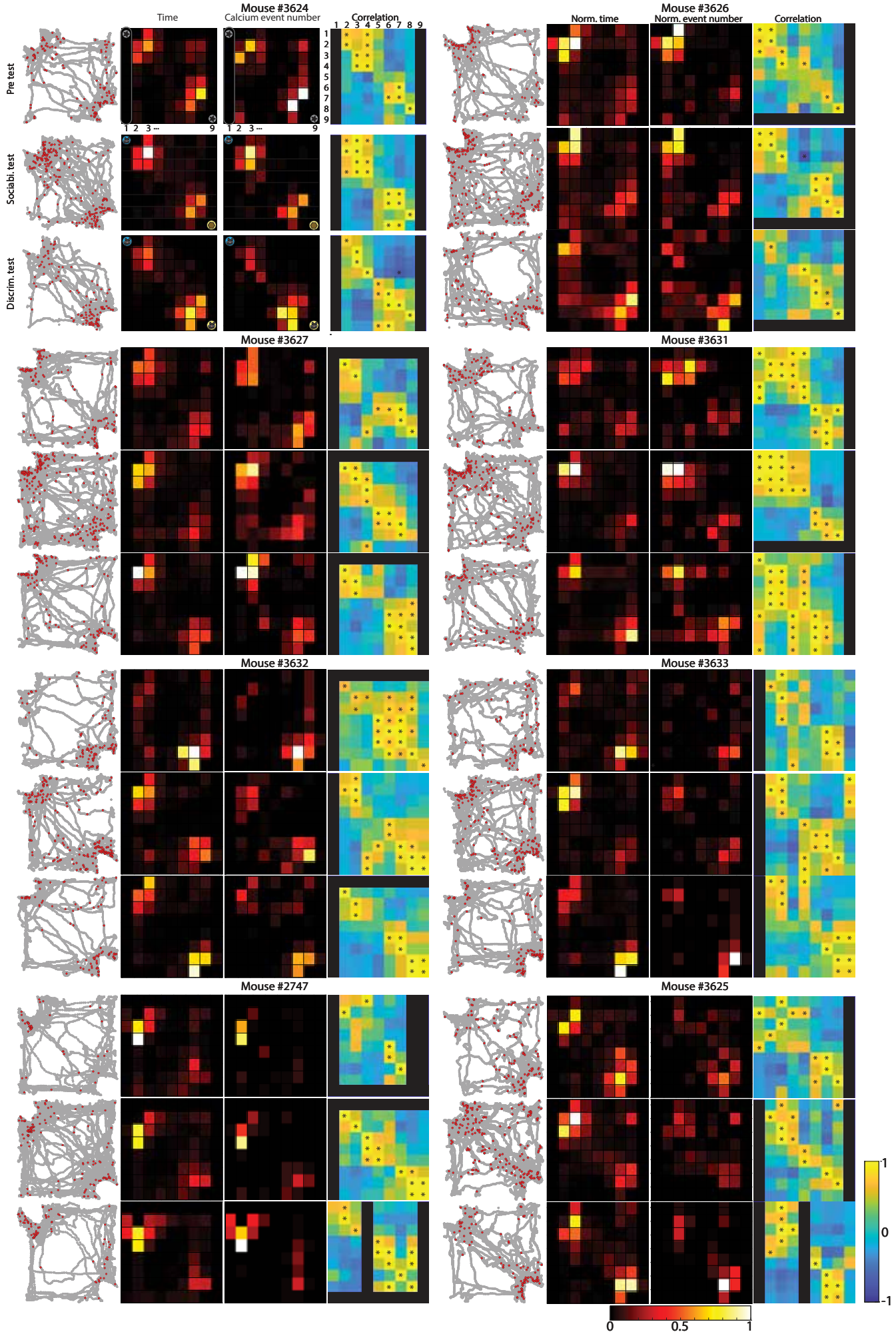
Mouse #3624
Time
Calcium event number
Correlation
Pre test
Sociabi. test
Discrim. test
Mouse #3626
Norm. time
Norm. event number
Correlation
Mouse #3627
Mouse #3631
Mouse #3632
Mouse #3633
Mouse #2747
Mouse #3625
0
0.5
1
-1
0
-1

Figure S7. Related to figure 7.

Maps of nose points (filled grey circles) and calcium events (filled red circles) in arena. Heat maps of the same data (but cumulative time and calcium event are separated) were also shown for each mouse (N = 8). Pearson's correlation coefficients with $p < 0.05$ is indicated by asterisk. All p values are presented in supplemental table.

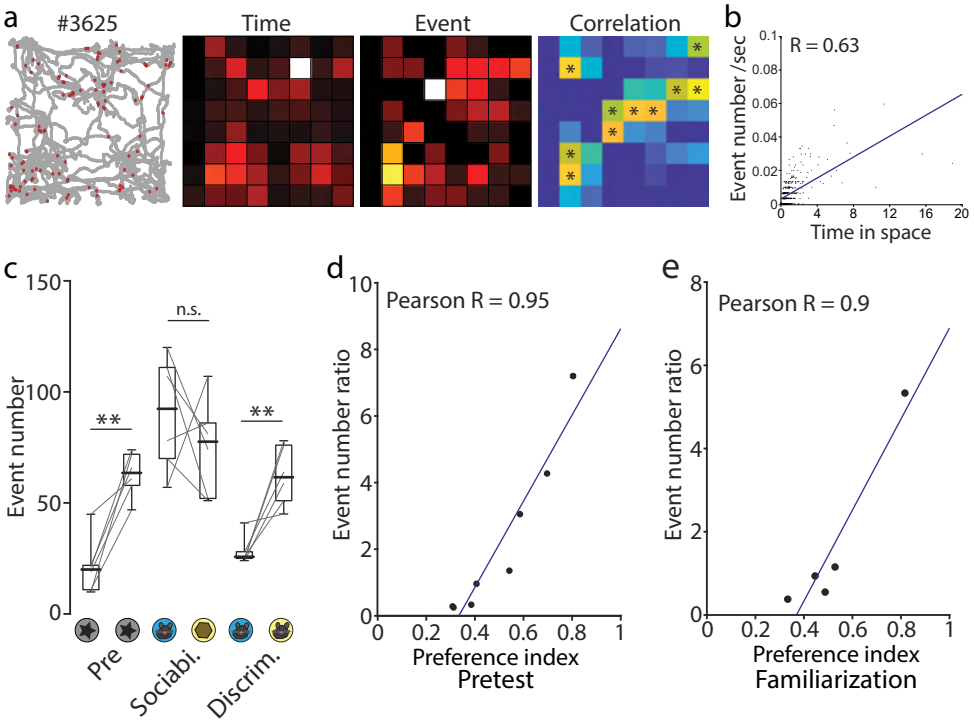

Figure S8. Related to figure 7.

(**a**) Example of maps of nose points and calcium events in open filed arena. (**b**) Correlation plots of event number and cumulative time in each pixels shown in **a**. $p < 0.001$, N = 7. (**c**) Box plots comparing a calcium event number when the mouse was in the interaction zones. In pretest, the object was aligned by longer interaction time (preffered object is plotted in right side).
Median event number: Pre (left vs right), 20 vs 63.5; Sociability (mouse vs object), 92.5 vs 77.5; Discrimination (familiar vs novel), 22.5 vs 61.5. $p = 0.001$, 0.385, and 0.006. Signed-rank test. N = 6. (**d and e**) Correlation plots of calcium event number ratios and preference index in pretest (**d**) and familiarization session (**e**). pretest, $p < 0.001$, N = 8; familiarization, $p = 0.014$, N = 5.

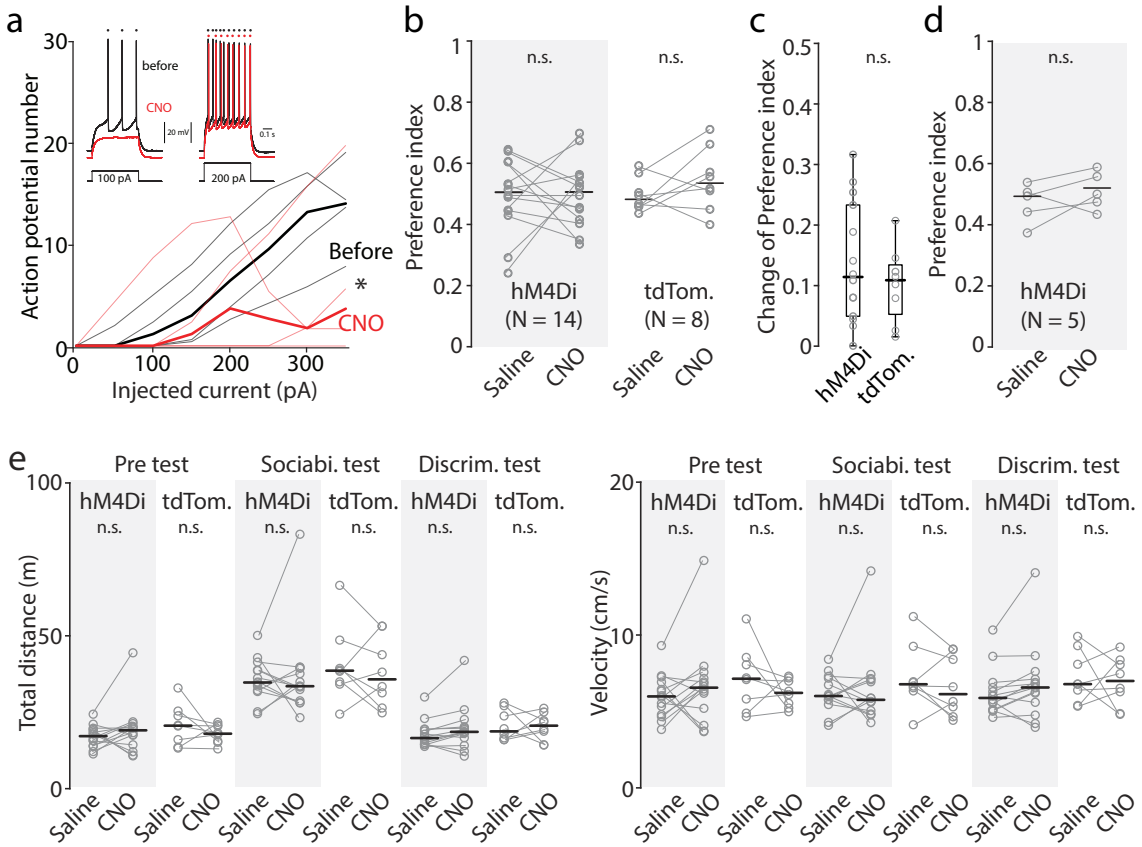

Figure S9. Related to figure 8.

(**a**) Frequency-current (FI) curves showing the effect of CNO on action potential number generated by current injection. Recordings were made from hM4Di expressing $EN^{vCA1\text{-}proj.}$ neurons before and after bath application of CNO (100 nM). Black line indicates before and red line indicates after CNO application. Inset: Traces showing spike response to 100 pA (left) and 200 pA (right) current injection. Saline vs CNO; F (1, 4.77) = 0.38, p = 0.0329, two-way ANOVA. n = 4 neurons. N = 2 mice. (**b**) Same as in **Fig. 8e**, but for preference index in pretest. Median preference index: hM4Di mice (Saline vs CNO), 0.5 vs 0.5, p = 0.92; signed-rank test; tdTomato mice (Saline vs CNO), 0.48 vs 0.53, p = 0.227; signed-rank test. (**c**) Absolute change of preference index before and after CNO treatment in hM4Di and tdTomato mice. Median change of preference index: hM4Di mice 0.11 (N = 14); tdTomato 0.11 (N = 8). hM4Di vs tdTomato, p = 0.517, ranksum test. (**d**) Same as in **b**, but for preference index in familiarization session of object recognition memory test. Median preference index: hM4Di mice (Saline vs CNO), 0.49 vs 0.5, p = 0.28; signed-rank test (**e**) Plots comparing locomotor activity (distance moved and velocity) for hM4Di and tdTomato mice under two different treatments. Median total distance: Pretest, hM4Di mice (Saline vs CNO), 17.17 vs 19.10, p = 0.426; tdTomato mice (Saline vs CNO), 20.60 vs 17.98, p = 0.25; Sociability test, hM4Di mice (Saline vs CNO), 34.72 vs 33.51, p = 0.855; tdTomato mice (Saline vs CNO), 38.59 vs 35.76, p = 0.547, Discrimination test, hM4Di mice (Saline vs CNO), 16.55 vs 18.58, p = 0.0676; tdTomato mice (Saline vs CNO), 18.73 vs 20.60, p = 0.945, all signed-rank test. Median velocity: Pretest, hM4Di mice (Saline vs CNO), 5.98 vs 6.55, p = 0.391; tdTomato mice (Saline vs CNO), 7.14 vs 6.21, p = 0.383; Sociability test, hM4Di mice (Saline vs CNO), 6.01 vs 5.76, p = 0.808; tdTomato mice (Saline vs CMO), 6.78 vs 6.13, p = 0.313; Discrimination test, hM4Di mice (Saline vs CNO), 5.88 vs 6.57, p = 0.104; tdTomato mice (Saline vs CNO), 6.79 vs 6.99, p = 0.945. All signed-rank test.

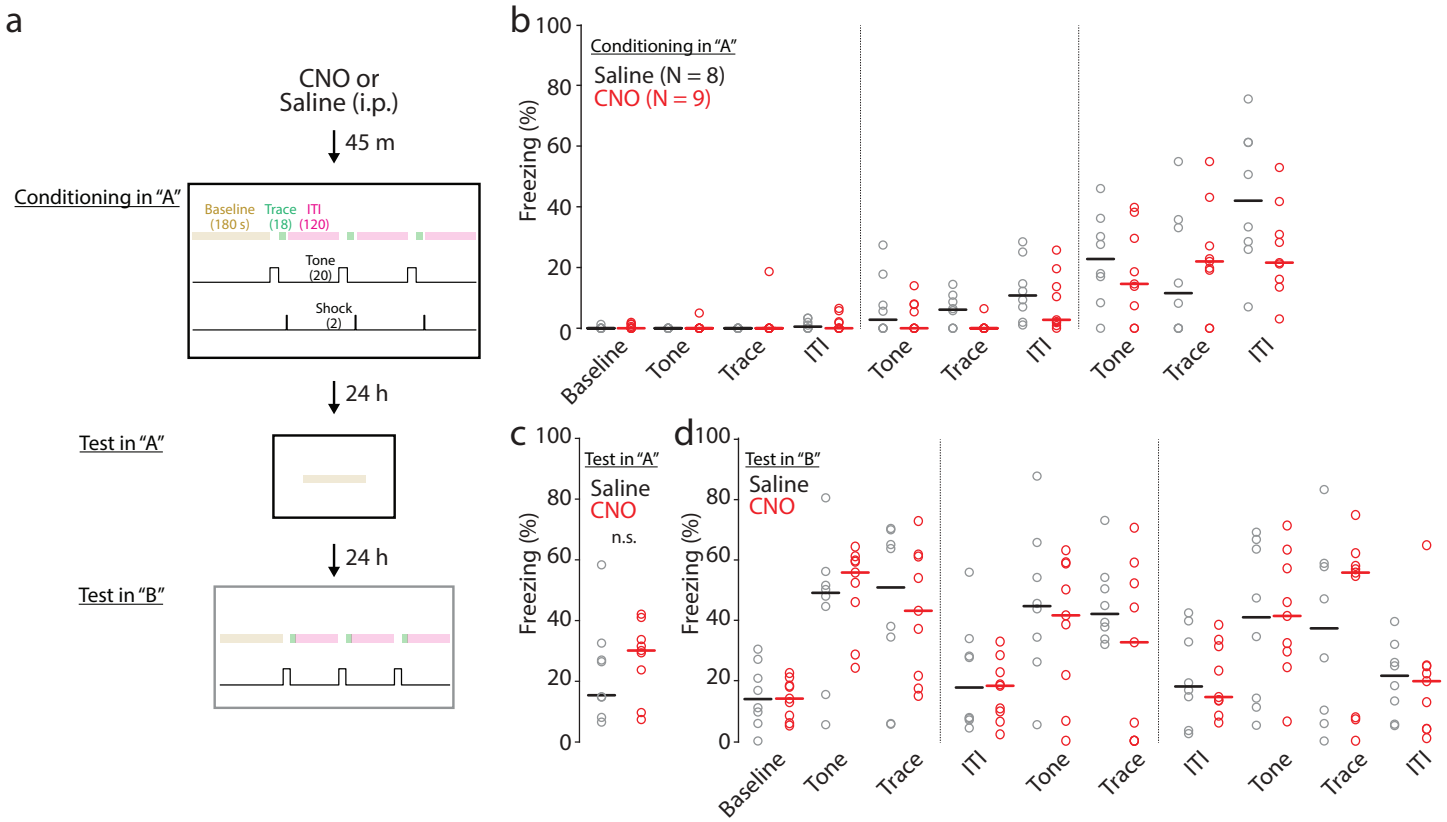

Figure S10. Related to figure 8.

(**a**) Schematic of trace fear conditioning protocol. (**b**) The effect of CNO on freezing behavior during conditioning. Black indicates saline treated group and red indicated CNO treated group. Data points of individual mice are indicated by empty circles. Thick horizontal bars indicate median values. Saline vs CNO, $F(1, 9) = 2.52$, $p = 0.115$; two-way ANOVA. (**c**) The effect of CNO on freezing behavior during recall to context "A". Median values of freezing %: Saline = 14.91, CNO = 30.13. Saline vs CNO, $p = 0.576$; one-way ANOVA. (**d**) The effect of CNO on freezing behavior during conditional stimulus recall in context "B". Saline vs CNO, $F(1, 9) = 0.38$, $p = 0.54$; two-way ANOVA.

Supplemental table_Fig6. d

Kruskal-Wallis ANOVA Table

Source	SS	df	MS	Chi-sq	Prob>Chi-sq
Columns	5936	7	848	30.3	8.36901e-05
Error	3272	40	81.8		
Total	9208	47			

Brain area		p value
insular	AOB	0.763868
insular	PIR	0.61693
insular	ENT	0.624003
insular	CLA	0.920835
insular	ENT	0.97145
insular	palidum	0.588459
insular	substantia innominata	0.439599
AOB	PIR	0.016481
AOB	ENT	0.999999
AOB	CLA	0.999975
AOB	EN	0.15622
AOB	palidum	0.999995
AOB	substantia innominata	0.999727
PIR	ENT	0.007706
PIR	CLA	0.048384
PIR	EN	0.993974
PIR	palidum	0.006377
PIR	substantia innominata	0.002784
ENT	CLA	0.999317
ENT	EN	0.091183
ENT	palidum	1
ENT	substantia innominata	0.999995
CLA	EN	0.316955
CLA	palidum	0.998784
CLA	substantia innominata	0.991761
EN	palidum	0.079439
EN	substantia innominata	0.042801
palidum	substantia innominata	0.999999

Supplemental table_Fig. S7

#3624_pre								
NaN	0.030466	0.063225	0.009075	0.247001	0.25055	0.49507	0.85628	NaN
NaN	0.009079	0.165818	0.014476	0.601503	0.360111	0.559533	0.8215	NaN
NaN	0.960633	0.007767	0.015595	0.292014	0.255931	0.372523	0.791749	NaN
NaN	0.912082	0.005971	0.002895	0.457643	0.343274	0.26234	0.893979	NaN
NaN	0.826345	0.507151	0.172157	0.409576	0.49807	0.291979	0.984138	NaN
NaN	0.795298	0.770565	0.541155	0.876885	0.05054	0.000408	0.525322	NaN
NaN	0.673628	0.681345	0.281931	0.670704	0.012283	0.009074	0.33916	NaN
NaN	0.397116	0.873865	0.500731	0.567492	0.44609	0.984597	0.000135	NaN
NaN	0.684599	0.702268	0.762463	0.432498	0.165201	0.453071	0.612292	NaN

#3626_pre								
6.17E-10	0.002565	0.271054	0.762518	0.287476	0.635151	0.872321	0.415415	NaN
0.019033	7.75E-05	0.517364	0.27832	0.630871	0.958205	0.604887	0.349523	NaN
0.00428	0.065322	0.016631	0.965173	0.064636	0.991044	0.944663	0.238115	NaN
0.479449	0.969113	0.00312	0.333624	0.031148	0.642773	0.809044	0.224346	NaN
0.096505	0.598858	0.267868	0.359752	0.264607	0.201098	0.531394	0.706396	NaN
0.845155	0.905673	0.48264	0.578133	0.348881	0.159276	0.121545	0.97373	NaN
0.519873	0.300624	0.857947	0.436932	0.273317	0.488053	0.031611	0.757087	NaN
0.828656	0.551477	0.451762	0.117931	0.152956	0.799032	0.404524	0.006236	NaN
NaN	NaN	NaN	NaN	NaN	NaN	NaN	NaN	NaN

#3624_social								
NaN	0.041978	0.000817	0.034955	1	0.738145	0.440428	0.767007	NaN
NaN	3.68E-05	0.000299	0.153722	0.517781	0.857114	0.395608	0.666533	NaN
NaN	0.078949	0.001226	0.011881	0.871199	0.589303	0.278125	0.602548	NaN
NaN	0.038606	0.001267	0.002458	0.816396	0.803494	0.296537	0.485362	NaN
NaN	0.738967	0.67764	0.249017	0.51719	0.771745	0.617633	0.933842	NaN
NaN	0.806401	0.467467	0.292532	0.26177	0.000236	0.002458	0.92883	NaN
NaN	0.666361	0.306487	0.140741	0.171752	0.001276	2.97E-05	0.422531	NaN
NaN	0.692917	0.357721	0.353016	0.240816	0.578525	0.311	9.37E-05	NaN
NaN	0.811081	0.607985	0.470149	0.289403	9.54E-06	0.00307	0.869896	NaN

#3626_social								
3.77E-07	0.006192	0.123932	0.493078	0.159001	0.943647	0.397797	0.699828	NaN
0.004005	0.000176	0.395232	0.739971	0.295457	0.868247	0.410544	0.506845	NaN
0.105691	0.425941	1.86E-06	0.552679	0.009065	0.78383	0.175885	0.315994	NaN
0.075199	0.334274	0.180009	0.803862	0.808609	0.919065	0.523503	0.259141	NaN
0.489975	0.282591	0.587152	0.65914	0.539794	0.00761	0.010367	0.658128	NaN
0.818835	0.569118	0.661017	0.847766	0.893176	2.95E-05	0.071781	0.893428	NaN
0.573783	0.452372	0.254822	0.449499	0.090618	0.125482	1.14E-06	0.091645	NaN
0.902498	0.707186	0.471821	0.322033	0.065942	0.727366	0.064039	7.39E-05	NaN
NaN	NaN	NaN	NaN	NaN	NaN	NaN	NaN	NaN

#3624_disc								
NaN	0.03002	0.14956	0.735765	0.533808	0.575455	0.412362	0.546207	NaN
NaN	0.170974	0.002239	0.493449	0.688509	0.324186	0.185075	0.363474	NaN
NaN	0.426759	0.000214	0.418802	0.539895	0.252658	0.0928	0.205829	NaN
NaN	0.213771	0.115009	0.00046	0.316029	0.158689	0.031734	0.149328	NaN
NaN	0.292298	0.536415	0.882683	0.033567	0.233292	0.872615	0.852812	NaN
NaN	0.964346	0.233191	0.372704	0.042495	2.81E-05	0.061553	0.292675	NaN
NaN	0.50164	0.152159	0.119264	0.245275	0.002404	0.000191	0.394057	NaN
NaN	0.978459	0.221689	0.23279	0.444032	0.117764	0.189503	0.000562	NaN
NaN	1	0.460032	0.448369	0.022306	0.00033	0.183628	0.472707	NaN

#3626_disc								
0.116854	0.428638	0.199432	0.221746	0.291077	0.64385	0.209412	0.318343	NaN
0.98509	0.03044	0.712253	0.434586	0.839962	0.724835	0.373537	0.916427	NaN
0.87982	0.118784	0.493003	0.804974	0.510575	0.407348	0.274831	0.920354	NaN
0.447491	0.962427	0.972214	0.074034	0.00118	0.300036	0.595149	0.072219	NaN
0.395494	0.495488	0.787993	0.476851	0.178069	0.011164	0.421436	0.45138	NaN
0.460788	0.634715	0.644964	0.832196	0.58497	0.000306	0.17159	0.728469	NaN
0.5414	0.842152	0.686763	0.680867	0.529838	0.003396	0.028034	0.421142	NaN
0.595461	0.787328	0.899922	0.084235	0.082273	0.723579	0.641754	0.000128	NaN
NaN	NaN	NaN	NaN	NaN	NaN	NaN	NaN	NaN

#3627_pre								
NaN	NaN	NaN	NaN	NaN	NaN	NaN	NaN	NaN
NaN	0.002118	0.09458	0.833916	0.848821	0.320206	0.436634	0.752715	NaN
NaN	0.08048	5.56E-05	0.84521	0.409013	0.401368	0.179675	0.525852	NaN
NaN	0.067913	0.062856	0.862424	0.736824	0.363912	0.243843	0.848574	NaN
NaN	0.316906	0.211822	0.622869	0.144195	0.231025	0.413674	0.35205	NaN
NaN	0.294663	0.208268	0.942777	0.038445	0.020527	0.002724	0.941711	NaN
NaN	0.433204	0.157074	0.232971	0.217805	0.115457	0.000543	0.164678	NaN
NaN	0.950899	0.482314	0.020065	0.824274	0.914082	0.310876	0.001427	NaN
NaN	0.678831	0.100405	0.595683	0.14277	0.52056	0.329521	0.958655	NaN

#3631_pre								
0.000326	0.213465	0.102416	0.002788	0.000641	0.73359	0.676674	0.554987	NaN
0.440927	0.002623	0.010173	0.015935	0.346164	0.656695	0.918679	0.328223	NaN
0.196195	0.00422	2.01E-05	0.004183	0.223081	0.663587	0.487087	0.312226	NaN
0.000848	0.622929	0.305357	0.037447	0.001632	0.749002	0.755794	0.598889	NaN
0.001871	0.9741	0.754082	0.230573	0.006906	0.479106	0.613586	0.980283	NaN
0.728356	0.188198	0.247074	0.270237	0.779693	0.00207	0.189816	0.004222	NaN
0.684454	0.599838	0.403058	0.813203	0.995183	0.46382	0.007583	0.590277	NaN
0.887409	0.783629	0.880909	0.921472	0.660669	0.037897	0.002284	0.108004	NaN
0.6703	0.679681	0.591141	0.889942	0.973646	0.465464	0.003321	0.605305	NaN

#3627_social								
NaN	NaN	NaN	NaN	NaN	NaN	NaN	NaN	NaN
NaN	3.66E-05	0.014207	0.623189	0.802708	0.977546	0.359923	0.34506	NaN
NaN	0.078083	0.002224	0.025879	0.902006	0.869705	0.374209	0.204548	NaN
NaN	0.382351	0.167226	0.00034	0.124891	0.269439	0.747726	0.389944	NaN
NaN	0.169543	0.069967	0.026351	0.152119	0.122461	0.495179	0.799283	NaN
NaN	0.764125	0.458902	0.729316	0.000972	0.003568	0.058924	0.978431	NaN
NaN	0.426506	0.250105	0.866129	0.036299	0.009818	0.001958	0.680055	NaN
NaN	0.498815	0.386031	0.783853	0.21157	0.102217	0.00607	0.052757	NaN
NaN	0.812556	0.456129	0.040977	0.781467	0.457873	0.603068	0.415659	NaN

#3631_social								
6.65E-07	0.001237	0.000279	0.137952	0.136543	0.806863	0.836424	0.834503	NaN
0.000325	1.4E-05	2.86E-07	0.036925	0.057915	0.779673	0.695408	0.80937	NaN
0.000315	0.004846	0.000581	0.12365	0.111344	0.687205	0.560697	0.708283	NaN
0.089755	0.010419	0.007702	0.004821	0.019638	0.459885	0.195264	0.586251	NaN
0.507158	0.596479	0.376542	0.266099	0.438329	0.851652	0.058153	0.354198	NaN
0.652793	0.355518	0.469017	0.589287	0.624506	0.026466	0.578966	0.675207	NaN
0.851279	0.546103	0.505103	0.382906	0.482245	0.012165	0.024376	0.263836	NaN
0.713801	0.743178	0.606889	0.437818	0.407994	0.501554	0.027055	0.000169	NaN
NaN	NaN	NaN	NaN	NaN	NaN	NaN	NaN	NaN

#3627_disc								
NaN	NaN	NaN	NaN	NaN	NaN	NaN	NaN	NaN
NaN	5E-06	0.054518	0.756265	0.110584	0.981268	0.317818	0.893604	NaN
NaN	0.016559	1.72E-05	0.398637	0.303666	0.487375	0.229246	0.869639	NaN
NaN	0.058502	0.004799	0.098995	0.092781	0.282179	0.491725	0.730481	NaN
NaN	0.815706	0.617524	0.40644	0.723685	0.260313	0.164761	0.029471	NaN
NaN	0.800146	0.390154	0.423394	0.71344	0.011865	0.019503	0.021017	NaN
NaN	0.521114	0.194279	0.615557	0.889438	0.001592	0.005724	0.204186	NaN
NaN	0.732882	0.51062	0.985348	0.936648	0.202704	0.014265	0.000118	NaN
NaN	0.672231	0.728533	0.939062	0.498386	0.207329	0.068338	0.004801	NaN

#3631_disc								
0.00018	0.510376	0.591451	0.26498	0.328068	0.196472	0.708096	0.458531	NaN
0.253429	8.59E-05	0.001814	0.421406	0.04077	0.980933	0.889777	0.333627	NaN
0.765937	0.007697	0.00592	0.608136	0.049357	0.650928	0.591501	0.51113	NaN
0.385461	0.000962	0.00471	0.133494	0.011766	0.630744	0.849828	0.765636	NaN
0.214457	0.000114	0.005071	0.103084	0.00115	0.498649	0.563547	0.812158	NaN
0.009424	0.228243	0.380863	0.001941	0.056828	0.006663	0.171832	0.912238	NaN
0.076096	0.812775	0.829994	0.014101	0.238719	0.001078	0.014742	0.633674	NaN
0.070759	0.861923	0.648363	0.009076	0.357756	2.48E-05	0.040725	0.408479	NaN
0.01669	0.908906	0.894298	0.032354	0.387424	0.004359	0.213	0.861524	NaN

#3632_pre								
NaN	NaN	NaN	NaN	NaN	NaN	NaN	NaN	NaN
NaN	0.010101	0.308861	0.269851	0.732413	0.95751	0.868795	0.22441	0.599092
NaN	0.338922	0.004661	0.029534	0.105161	0.013031	0.066348	0.02131	0.821595
NaN	0.09491	0.042843	0.184365	0.056229	0.000814	0.013303	0.00048	0.878763
NaN	0.331771	0.779156	0.765231	7.77E-07	0.005307	2.11E-05	0.089383	0.568267
NaN	0.280597	0.589818	0.768696	0.000969	3.24E-07	5.06E-06	0.003929	0.897015
NaN	0.545783	0.808396	0.70321	6.93E-12	0.002358	2.74E-09	0.08355	0.957354
NaN	0.337561	0.439578	0.856045	0.200022	4.28E-05	0.016576	1.22E-09	0.066664
NaN	0.463876	0.203817	0.193748	0.667272	0.312951	0.815796	0.071586	0.001433

#3633_pre								
NaN	0.628577	0.000386	0.219944	0.628577	0.469044	0.574327	0.587245	0.334069
NaN	0.033385	0.257961	0.836155	0.068272	0.513549	0.843015	0.937469	0.470028
NaN	0.687039	0.000742	0.093894	0.487565	0.497529	0.586758	0.534473	0.461079
NaN	0.871404	0.078956	0.639839	0.086738	0.20235	0.571631	0.738171	0.883587
NaN	0.91364	0.016072	0.521823	0.052541	0.696771	0.672394	0.898877	0.509578
NaN	0.737077	0.528113	0.259129	0.989763	0.456884	0.003312	0.158793	0.128698
NaN	0.887303	0.49753	0.385922	0.800584	0.545731	2.28E-06	0.021092	0.164018
NaN	0.518456	0.967411	0.160231	0.467595	0.649254	0.015255	0.000202	0.375018
NaN	0.902209	0.897506	0.027463	0.79744	0.58995	0.192055	0.026482	0.748216

#3632_social								
NaN	0.11584	0.021093	0.823881	0.892166	0.649724	0.709718	0.665195	0.735765
NaN	0.015828	0.000118	0.561795	0.850463	0.901207	0.545812	0.539581	0.647718
NaN	0.255393	0.006838	0.609497	0.73509	0.819514	0.439611	0.851789	0.949352
NaN	0.710052	0.108747	0.278363	0.9622	0.711859	0.820725	0.791103	0.746397
NaN	0.678071	0.915926	0.71403	0.477035	0.019659	0.205044	0.167218	0.158886
NaN	0.686032	0.854663	0.420515	0.510254	0.024402	0.115097	0.068005	0.076385
NaN	0.608063	0.288936	0.369152	0.019458	0.367044	3.27E-06	0.025032	0.192219
NaN	0.643435	0.385247	0.024456	0.10538	0.853128	0.010529	1.75E-05	0.009032
NaN	0.772301	0.470824	0.009272	0.628283	0.924994	0.220565	0.00071	3.31E-05

#3633_social								
NaN	0.054622	0.000543	0.523221	0.234824	0.983431	0.492745	0.793155	9.38E-11
NaN	5.63E-06	0.019031	0.785215	0.78174	0.560888	0.63261	0.600986	0.079461
NaN	0.075009	0.00056	0.692938	0.581425	0.499455	0.349772	0.815497	0.009674
NaN	0.541701	0.047572	0.318044	0.962795	0.156367	0.203607	0.619359	0.115239
NaN	0.879689	0.828902	0.730351	0.026498	0.357639	0.071063	0.270119	0.577714
NaN	0.457046	0.637704	0.268299	0.250239	0.013252	0.007237	0.643737	0.940217
NaN	0.293527	0.315236	0.08286	0.232302	0.01922	0.000566	0.295837	0.503708
NaN	0.870744	0.990169	0.277585	0.007866	0.443784	0.135116	0.000474	0.93126
NaN	0.8279	0.47373	0.532282	0.006046	0.316508	0.048388	0.122135	0.381473

#3632_disc								
NaN	NaN	NaN	NaN	NaN	NaN	NaN	NaN	NaN
NaN	0.000166	0.607484	0.812085	0.834638	0.757625	0.679918	0.565224	0.506887
NaN	0.285775	0.008472	0.114384	0.470553	0.487474	0.412719	0.957179	0.687417
NaN	0.212972	0.00513	0.069921	0.596291	0.850635	0.577972	0.76919	0.459523
NaN	0.935203	0.707939	0.63543	0.638686	0.212526	0.074291	0.962248	0.762442
NaN	0.641247	0.631533	0.985765	0.723457	0.00884	0.002462	0.098147	0.107022
NaN	0.542319	0.294154	0.432876	0.628158	0.168295	0.000242	0.345261	0.347587
NaN	0.573811	0.517008	0.627367	0.279017	0.566376	0.130992	3.93E-05	0.004354
NaN	0.475508	0.550939	0.652814	0.303768	0.588048	0.134303	2.91E-05	0.002157

#3633_disc								
NaN	0.000279	0.028012	0.843572	0.002579	0.635037	0.66811	0.616677	0.632806
NaN	0.089901	0.025009	0.712377	0.053334	0.975738	0.477854	0.674199	0.709573
NaN	0.165271	0.008575	0.241094	0.052064	0.561081	0.595882	0.9294	0.815583
NaN	0.390222	0.062839	0.825493	0.216764	0.939077	0.213225	0.96664	0.998884
NaN	0.478871	0.427891	0.375636	0.640491	0.053025	0.959674	0.084598	0.114479
NaN	0.98912	0.793391	0.954408	0.851337	0.255477	0.139524	0.004351	0.003354
NaN	0.683569	0.653767	0.486583	0.607857	0.99537	3.4E-05	0.340287	0.240069
NaN	0.81734	0.918257	0.998433	0.735212	0.483421	0.358025	5E-06	0.000326
NaN	0.254154	0.122219	0.586417	0.264955	0.711655	0.407609	0.015599	0.015378

#2747_pre								
NaN	0.076345	0.115679	0.005031	0.568779	0.533279	0.678195	NaN	NaN
NaN	0.002602	0.985529	0.505889	0.74841	0.91108	0.510368	NaN	NaN
NaN	0.572814	0.101934	0.219095	0.545701	0.396636	0.373131	NaN	NaN
NaN	0.824664	0.065901	0.558511	0.613663	0.648751	0.636674	NaN	NaN
NaN	0.723126	0.094889	0.981534	0.91555	0.000845	0.605363	NaN	NaN
NaN	0.954504	0.804884	0.548681	0.45694	0.013694	0.418917	NaN	NaN
NaN	0.400426	0.332966	0.651164	0.544412	0.824315	2.52E-07	NaN	NaN
NaN	0.849618	0.7916	0.753061	0.484867	0.077418	0.406677	NaN	NaN
NaN	NaN	NaN	NaN	NaN	NaN	NaN	NaN	NaN

#3625_pre								
0.608727	0.850559	0.003368	0.960074	0.636616	0.976302	0.527234	0.685799	NaN
0.000106	0.149291	0.541367	0.013292	0.038595	0.363184	0.577025	0.366128	NaN
0.495397	0.808056	0.00051	0.818595	0.691534	0.914389	0.548412	0.535574	NaN
0.314188	0.015343	0.242964	0.312146	0.443042	0.662345	0.26439	0.284593	NaN
0.018246	0.885017	0.254426	0.074357	0.085637	0.967009	0.858292	0.982732	NaN
0.466687	0.37978	0.389352	0.641248	0.264786	0.020249	0.000471	0.363818	NaN
0.446308	0.243674	0.102623	0.927605	0.393258	0.135606	0.001547	0.241966	NaN
0.517818	0.358923	0.389698	0.895968	0.61709	0.041569	0.544864	2.54E-05	NaN
0.539106	0.372273	0.157004	0.698802	0.949781	0.105828	0.86565	0.296466	NaN

#2747_social								
NaN	NaN	NaN	NaN	NaN	NaN	NaN	NaN	NaN
NaN	0.000627	0.165924	0.753616	0.441708	0.484072	0.554233	0.3782	0.617625
NaN	0.064899	0.001375	0.748646	0.949441	0.133493	0.267859	0.360193	0.787433
NaN	0.240102	0.813823	3.16E-05	0.078765	0.100386	0.941222	0.437691	0.743508
NaN	0.653408	0.80297	0.001756	0.018784	0.249087	0.433565	0.723764	0.791436
NaN	0.382912	0.949077	0.036206	0.00525	0.101968	0.379665	0.783105	0.68411
NaN	0.468297	0.319527	0.463549	0.628766	0.710327	0.00191	0.02346	0.162982
NaN	0.475538	0.448768	0.625299	0.892958	0.519101	0.225407	6.54E-05	0.000314
NaN	0.813281	0.493207	0.920044	0.908011	0.217971	0.368696	0.002235	3.66E-05

#3625_social								
NaN	0.969814	0.026899	0.351813	0.519536	0.8415	0.469098	0.042041	NaN
NaN	0.004721	0.06351	0.021604	0.371832	0.379606	0.26096	0.905174	NaN
NaN	0.474202	0.000193	0.10028	0.259392	0.791189	0.260075	0.273276	NaN
NaN	0.266627	0.00027	0.035775	0.399139	0.728065	0.14716	0.511406	NaN
NaN	0.829272	0.556395	0.107856	0.037249	0.350233	0.539001	0.964042	NaN
NaN	0.9005	0.763285	0.533817	0.006865	0.060874	0.250035	0.580278	NaN
NaN	0.293168	0.354083	0.185762	0.951668	0.869825	0.002034	0.18721	NaN
NaN	0.735042	0.537674	0.940858	0.660768	0.137948	0.089627	0.00412	NaN
NaN	0.352813	0.376697	0.781705	0.332896	0.572982	0.478068	0.667675	NaN

#2747_disc								
0.079098	0.041108	0.38234	NaN	0.861498	0.962905	0.657805	0.955684	NaN
0.283395	0.00352	0.222227	NaN	0.61776	0.41489	0.429246	0.411609	NaN
0.582595	0.287462	0.0366	NaN	0.560442	0.87244	0.321495	0.887725	NaN
0.443603	0.365645	0.869849	NaN	0.013604	0.090606	0.532438	0.100124	NaN
0.483119	0.338392	0.405255	NaN	0.001247	0.000238	0.915131	0.000374	NaN
0.638186	0.296286	0.237713	NaN	0.248619	0.003016	0.24172	0.002287	NaN
0.421699	0.829495	0.307739	NaN	0.55076	0.634139	6.4E-05	0.604193	NaN
0.400059	0.272354	0.306505	NaN	0.187301	0.000648	0.5387	0.000417	NaN
NaN	NaN	NaN	NaN	NaN	NaN	NaN	NaN	NaN

#3625_disc								
NaN	0.296586	0.000596	0.080166	NaN	0.531817	0.474728	0.447723	0.6086
NaN	0.058684	0.044706	0.649261	NaN	0.855447	0.45265	0.500144	0.69241
NaN	0.557906	0.000328	0.003232	NaN	0.342664	0.326653	0.20977	0.619682
NaN	0.065285	0.010373	0.369174	NaN	0.692956	0.652509	0.539011	0.719256
NaN	0.04167	0.229085	0.770469	NaN	0.205574	0.146091	0.193319	0.280255
NaN	0.761387	0.392216	0.643809	NaN	0.000137	0.651962	0.486404	0.074555
NaN	0.295644	0.156373	0.265812	NaN	0.328568	0.000181	0.061121	0.543931
NaN	0.390951	0.231408	0.345861	NaN	0.829137	0.00263	0.00083	0.706393
NaN	0.542932	0.36326	0.443115	NaN	0.563435	0.000168	0.032326	0.819186

Supplemental table_Fig. S8a								
	NaN	0.288478	0.596444	0.865819	0.668025	0.75739	0.558572	0.596858
	NaN	0.004295	0.365154	0.760617	0.308386	0.89982	0.480338	0.843133
	NaN	0.033724	0.161321	0.783996	0.366506	0.748945	0.472526	0.391075
	NaN	0.469768	0.833893	0.008743	0.418076	0.480572	0.603412	0.523273
	NaN	0.266863	0.689468	0.047059	0.006025	0.008799	0.483023	0.440636
	NaN	0.758606	0.987706	0.855823	0.182081	0.204567	0.03272	0.00037
	NaN	0.002515	0.27312	0.96463	0.201806	0.880199	0.872272	0.97487
	NaN	0.282843	0.710085	0.512635	0.705534	0.62562	0.279554	0.04884